AD-A113 654 MATERIALS SCIENCES CORP SPRING HOUSE PA F/G 11/4
RESEARCH STUDY TO DEFINE THE CRITICAL FAILURE MECHANISMS IN NOT--ETC(U)
MAR 81 B W ROSEN, A P NAGARKAR, R B PIPES N00019-79-C-0633
UNCLASSIFIED MSC/TFR/1201/1801 NL

1 OF 2
AD A
113654

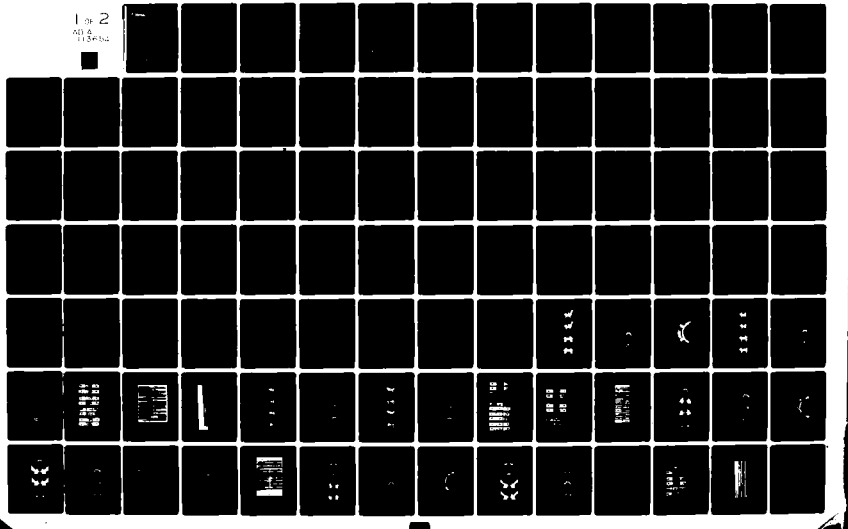

Materials Sciences Corporation

RESEARCH STUDY TO DEFINE THE CRITICAL FAILURE MECHANISMS IN NOTCHED COMPOSITES UNDER COMPRESSION FATIGUE LOADING

B. W. ROSEN, A. P. NAGARKAR, R. B. PIPES AND R. WALSH

NAVAL AIR SYSTEMS COMMAND
WASHINGTON, DC

MSC TFR 1201/1801
MARCH, 1981

CORRECTION PAGE

UNCLASSIFIED

SECURITY CLASSIFICATION OF THIS PAGE (When Data Entered)

REPORT DOCUMENTATION PAGE		READ INSTRUCTIONS BEFORE COMPLETING FORM
1. REPORT NUMBER MSC TFR 1201/1801	2. GOVT ACCESSION NO. AD-A113 654	3. RECIPIENT'S CATALOG NUMBER
4. TITLE (and Subtitle) Research Study to Define the Critical Failure Mechanisms in Notched Composites Under Compression Fatigue Loading		5. TYPE OF REPORT & PERIOD COVERED Final Report Sept. 1979 - March 1981 6. PERFORMING ORG. REPORT NUMBER
7. AUTHOR(s) B. W. Rosen, A. P. Nagarkar R. B. Pipes and R. Walsh		8. CONTRACT OR GRANT NUMBER(s) N00019-79-C-0633
9. PERFORMING ORGANIZATION NAME AND ADDRESS Materials Sciences Corporation Gwynedd Plaza II, Bethlehem Pike Spring House, PA 19477		10. PROGRAM ELEMENT, PROJECT, TASK AREA & WORK UNIT NUMBERS
11. CONTROLLING OFFICE NAME AND ADDRESS Naval Air Systems Command Washington, DC 20361		12. REPORT DATE March, 1981 13. NUMBER OF PAGES 113
14. MONITORING AGENCY NAME & ADDRESS(if different from Controlling Office)		15. SECURITY CLASS. (of this report) Unclassified 15a. DECLASSIFICATION DOWNGRADING SCHEDULE

16. DISTRIBUTION STATEMENT (of this Report)

Approved for Public Release; Distribution Unlimited.

17. DISTRIBUTION STATEMENT (of the abstract entered in Block 20, if different from Report)

18. SUPPLEMENTARY NOTES

19. KEY WORDS (Continue on reverse side if necessary and identify by block number)

Composites
Compression
Fatigue
Laminates
Stress Correlations

20. ABSTRACT (Continue on reverse side if necessary and identify by block number)

Analytical and experimental studies have been performed to examine the effects of stacking sequence and matrix material on damage growth and failure mechanisms in Graphite/Epoxy composites subjected to compression fatigue. Both fiber dominated and quasi-isotropic laminates are considered. Ultrasonic C-scans and photomicrographic studies have been utilized to observe interlaminar disbonds as well as intralaminar (Over)

DD FORM 1 JAN 73 1473 EDITION OF 1 NOV 65 IS OBSOLETE

SECURITY CLASSIFICATION OF THIS PAGE (When Data Entered)

CORRECTION PAGE

UNCLASSIFIED

SECURITY CLASSIFICATION OF THIS PAGE(When Data Entered)

Block 20 cont.

crack growth. A quasi-static finite element analysis has been performed by modeling the laminate as an assemblage of membrane elements connected by shear springs which allow load transfer through the thickness. Interlaminar and intralaminar failures for each step increase in load have been predicted by the use of appropriate failure criteria and use of iterative techniques. The effect of fatigue has been considered in terms of assumed degradations in matrix dominated strength characteristics. Correlation of analytical results and experimental data has been attempted and the reasons for various failure modes have been examined. Results of a simple analysis to study the possibility of buckling of delaminated surface plies in quasi-isotropic laminates are also reported.

SUMMARY

Analytical and experimental studies to identify the dominant failure mechanisms for compression fatigue of notched composite laminates have been conducted. The effects of stacking sequence and matrix material on damage growth as well as failure mechanisms under compression fatigue loading are reported. Two types of resin materials and four kinds of laminate layups have been considered. Two of the stacking sequences are fiber dominated and two are quasi-isotropic. Ultrasonic C-scans and photomicrographic studies have been utilized for experimental observations. An analytical methodology developed for the study of tension fatigue of notched laminates has been modified to obtain patterns of damage growth under quasi-static load by increasing it gradually in steps. For each step increase in load, a finite element stress analysis is performed and intralaminar and/or interlaminar failures in the elements are predicted. Stiffnesses of failed elements are adjusted to include the effects of damages. The finite element model consists of membrane elements representing the laminae and shear spring elements which transfer load between a laminae. Cyclic loading usually degrades the matrix dominated strengths. Due to the absence of experimental data on such degradation, some assuptions are made to obtain the degraded strength characteristics. Correlations of analytical results and experimental data are attempted and the reasons for various failure modes are critically examined.

Failure of quasi-isotropic laminates is observed to be dominated by growth of delaminations and consequent buckling of unsupported surface plies. A simplified analysis has been performed to study the interlaminar disbond as well as possibility of buckling modes. Final failure of fiber dominated laminates seems to occur as a result of significant intralaminar damages in the $\pm 45°$ plies. Changing the matrix material from a 5208 epoxy resin to a 5209 resin system does not appear to have any effect on the damage patterns and failure mechanisms, but may result in some differences in residual strength and/or lifetime.

FOREWORD

This report summarizes the work accomplished by the Materials Sciences Corporation (MSC) under Naval Air Systems Command (NASC) Contract No. N00019-79-C-0633. Dr. D. Mulville was the NASC Contract Monitor. The authors also acknowledge valuable technical discussions held with Dr. A. Somoroff of NASC.

The Project Manager and Principal Investigator for MSC were Dr. B. W. Rosen and Mr. A. P. Nagarkar, respectively. The experimental program was conducted at the University of Delaware under the supervision of Dr. R. B. Pipes. The authors express their appreciation to Dr. S. N. Chatterjee for his technical assistance during the later stages of this program.

Approved by:

B. Walter Rosen
President

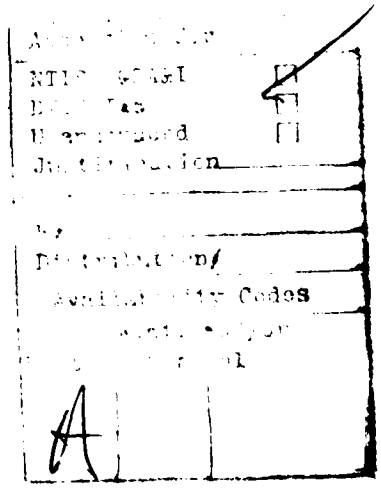

TABLE OF CONTENTS

LIST OF TABLES

LIST OF FIGURES

LIST OF FIGURES (Continued)

LIST OF FIGURES (Continued)

LIST OF FIGURES (Concluded)

INTRODUCTION

Efficient utilization of composite materials for primary aerospace structural applications requires evaluation of strength as well as lifetime of such materials under all anticipated environments. This necessitates the development of a broad experimental data base to characterize their properties under static as well as cyclic loading, and a fundamental understanding of the mechanisms of failure. A number of recent studies have been conducted with such objectives, and the results indicate that the effect of fatigue is most critical for structures under compressive loads, and significant amounts of damage are generated before failure under quasi-static or cyclic loading. The objective of the present study is to identify the dominant failure mechanisms for compression fatigue of a laminate containing a hole. The emphasis is upon understanding the governing physical phenomena. Accordingly, the experimental tasks were exploratory in nature and the analytical tasks were at a preliminary design level.

The program plan was based upon the hypothesis that matrix properties and interlaminar stresses have significant effects upon the failure process for cyclic compression loads. Hence, alternate matrix materials and different laminate configurations and stacking sequences were considered, both experimentally and analytically. The overall program is outlined in the "Background and Approach" section.

BACKGROUND AND APPROACH

The current state of the art in life prediction methodologies of composite structural elements has been reviewed in references 1 and 2, where the commonly observed sequences of various damage growth mechanisms have also been discussed. These discussions indicate that intralaminar damages, usually in the form of cracks parallel to the fibers, are the first to initiate in some of the laminae. As load cycling continues (or the static load is increased) these intralaminar cracks grow into interlaminar disbonds. For the case of cyclic loading the complexity of damage growth mechanisms is increased because of degradations in residual strength. In the case of a notched laminate the residual strength of the laminate as a whole can sometimes increase because of reduction in stress concentration due to intralaminar cracking. Consideration of changes in residual strength as well as simultaneous modeling of growth of all kinds of damage pose a difficult problem. Modeling of intralaminar damage growth as well as strength degradation has been attempted in reference 3 for correlation with experimental data. Growth of inherent interlaminar disbonds has been modeled in reference 4 by the use of semi-empirical self similar crack growth laws which are commonly used for metals. A "wearout" type model to predict residual strength and/or lifetime based on buckling of the delaminated plies has also been attempted in reference 4 for data correlation purposes. An attempt to model changes in residual strength as well as growth of intralaminar and interlaminar damage is reported in references 5 and 6. These studies clearly show two major problems with which one has to deal in modeling damage growth. The first problem is that practically no data base exists for the changes in residual strengths of the unidirectional lamina under tension and compression (in longitudinal and transverse directions) as well as shear. Interlaminar strengths may also degrade under cyclic loading. The second problem is the complexity involved in stress analysis in the presence of both intralaminar and interlaminar damages. The solution to the

first problem can be obtained by a comprehensive test program. Alternatively, limited test data and reasonable estimation procedures (linear residual strength reduction, as an example) may be utilized.

The stress analysis problem discussed above can possibly be handled by the use of specialized finite element formulations. One such attempt is described in reference 7, where it has been shown that fiber breakage, matrix crazing, crack bridging, matrix fiber debonding and axial splitting can occur near a built-in flaw in a unidirectional composite during quasi-static loading prior to catastrophic fracture. Use of this model for studying damage growth in laminated composites is likely to be too cumbersome as well as expensive and has not been attempted to date. For compression loads such micromechanical models should also include the effects of imperfections and the possibility of "microbuckling" of fibers. For the study of laminated composites, use of 3-D finite elements has been attempted in the past. Modeling each lamina as an assembly of plate type elements may also be attempted. Modeling damage growth requires the use of an iterative technique and therefore use of 3-D brick elements or plate elements becomes an expensive proposition. For many types of laminates subjected to extensional loadings, effects of normal displacements can often be neglected and in such cases each lamina can be modeled using membrane elements to depict the in-plane response. Such an approach has been utilized in reference 8, where the nodes in adjacent laminae are assumed to be connected by shear springs, which are assumed to be rigid under extension. Stiffnesses of the springs are calculated from the interlaminar shear moduli. To model damage growth under quasi-static loading of notched laminates, the model is loaded in steps and after each step appropriate stiffnesses of each element are reduced if failure is expected in a particular mode, and the load is recalculated in an iterative fashion. To consider load cycling effects in tension fatigue, use is made of assumed degradation characteristics of each strength parameter. An iterative technique is again used for number of cycles. The computer code

FLAC, developed in reference 8, has been utilized in this study after some modifications. Effects of load cycling are not considered in much detail, since no data are available regarding strength degradation, but a damage state is predicted for quasi-static loading. Some matrix dominated strength parameters are arbitrarily reduced to consider matrix degradation due to cyclic loading. Detailed discussions on advantages and shortcomings of the methodology are presented in the next section. Since cumulative damage due to load cycling is not included, the results are qualitative in nature and have been used to observe trends when correlating with experimental data.

To check the validity of the assumptions and gain insight into the different failure mechanisms involved, a series of experiments has been conducted on inch-wide specimens. Stress concentrations have been introduced into the specimens in the form of notches to accelerate the initiation and growth of fatigue damage. Key variables in the experimental program have been the matrix material, load and fatigue cycle levels, laminate configuration and stacking sequence. Two stacking sequences of the $[0_2/\pm 45]_{5s}$ and the $[0/\pm 45/90]_{5s}$ laminates fabricated from T-300/5208 and T-300/5209 Graphite/Epoxy have been used in the fatigue testing. The phenomena which have been studied are: (i) initiation and growth of fatigue damage; (ii) fatigue life and mode of fatigue failure; and (iii) residual strength and mode of static failure after a predetermined number of fatigue cycles. Ultrasonic C-scan techniques and photomicrography have been utilized to check for fatigue damage at different load cycle levels. The experimental program is described in the section "Experimental Program" and the results are presented in the section "Results and Correlation Studies."

Delamination of surface plies and their subsequent buckling have been observed to be one of the modes of failure. To study this in some detail, a buckling analysis of orthotropic plates with various boundary conditions has been conducted in conjunction with a lamination theory analysis to correlate the average laminate load to critical buckling loads for delaminated plies and delaminated areas. These results are presented in the section "Buckling Analysis."

ANALYTICAL METHODOLOGY

A "mini-mechanics" type of model is utilized herein to study progressive damage growth in laminated composites by considering the interactions of the response of the individual plies and failure mechanisms like matrix failure and ply disbonding, etc. Stress analysis in the presence of various damage modes is carried out in an iterative manner. The methodology consists of a finite element stress analysis and a failure analysis, which are discussed in the next two subsections. A detailed study of load cycling effects is not considered, but an attempt is made to determine effects of degradation of matrix material in each lamina and strength characteristics of the interfaces because of fatigue. However, use can be made of a fatigue analysis methodology similar to the ones utilized in references 5, 6, and 8, to consider effects of load cycling on gradual strength degradation. The approach has the ability to predict the various types of damages which may occur in reality, in contrast to other deterministic or probabilistic life prediction methodologies based on strength degradations of a component which are to be determined from test data.

STRESS ANALYSIS

In the present study the laminate is modeled with:

1. Membrane elements, used to represent the individual plies - They are quadrilateral plane stress elements with orthotropic elastic properties.
2. Beam elements, used to represent the ply interfaces - They do not have any axial displacements, and have orthotropic elastic properties. The moment of inertia of the cross section is adjusted to obtain the necessary shear displacement from the beam bending stiffness. The beams thus act as shear springs.

The notched laminate structure is assembled from these elements (fig. 1). Element stiffnesses are generated assuming kinematically admissible displacement fields and applying the principle of Minimum Potential Energy.

The validity of the present model and the resulting stress distribution have been compared, in reference 8, with a finite difference analysis of the free edge effects problem (ref. 9) for a $[\pm 45]_s$ laminate and a quasi three-dimensional analysis (ref. 10) for a $[\pm 30/90]_s$ laminate. Since this comparison indicates some important characteristics, it is reproduced here in figures 2 and 3. The correlation in the stresses predicted by the present model and the other two analyses is extremely good. The only significant difference is that while the quasi three-dimensional analysis yields $\sigma_{yz} = 0$ at $y/b = 1$, the present model does not. The present model cannot predict the interlaminar normal stress. An attempt has been made, in reference 8, to calculate this stress using equilibrium equations and the predicted stresses. Such a calculation should meet the force equilibrium requirement in the z-direction $\int_0^b \sigma_{zz} dz = 0$, i.e. positive and negative areas of the σ_{zz} curve (fig. 4) must be equal. This requirement is not met. The reason for this is the fact that although overall force equilibrium in the z-direction is satisfied in the model because of the nature of the problem, no requirement is imposed to satisfy such a condition at each node. In fact displacement (in z-direction) constraints are specified at each node only by demanding that shear springs are rigid in the axial direction. This difficulty can be overcome by using springs with finite stiffnesses in z-direction, but the membrane elements can no longer be utilized and use of plates will become necessary. This will make the analysis more expensive, as discussed in the Introduction. Normal stresses (σ_{zz}) are therefore not calculated, but the interlaminar strength used in the failure analysis is decreased to account for the effect of interlaminar normal stresses on interface failure. Such an approach appears adequate since this is a preliminary study, with

qualitative correlation to be made with experiments. For a more detailed quantitative analysis, use of a more sophisticated model capable of predicting the interlaminar normal stress may be necessary. Other details of the finite element analysis can be found in reference 8.

FAILURE ANALYSIS

The second requirement in the analysis is prediction of the load at which the different elements in the model will fail. Composite laminates can fail in various modes, hence different failure criteria are required to determine the likely mode of failure. The criteria used are presented in table 1. These criteria deal essentially with three types of failure: matrix and fiber failure in a lamina, and interlaminar failure. In-plane (lamina) and interlaminar failures are assumed to have no interaction; i.e. only the in-plane stresses are involved in in-plane failure mechanisms and the interlaminar failure results only due to interlaminar shear and normal stresses.

The failure analysis methodology is outlined in figure 5. In every load step, stresses are calculated with a finite element analysis for a unit load. For each element, assuming linear elastic behavior, failure load ratios are calculated from the stress distribution and all the failure criteria. The least ratio is determined and the element is predicted to fail in the appropriate failure mode. The least failure loads are compared to the actual applied load and the element or elements that have failed are identified. The possibility of gross laminate failure is then examined. If such a possibility does not exist, loss of strength and stiffness of failed elements is reflected in the next step by drastically reducing the stiffnesses and load-carrying capacity. The iterations can be carried out until the laminate fails.

The compressive nature of the loading complicates the failure problem with additional failure mechanisms that are primarily

structural in nature, rather than intrinsic material behavior. However, the failure criteria used in this and other studies are dependent only on material properties. This study attempts to overcome the structural instability problem by conducting a separate plate buckling analysis, which is discussed in a later section.

Load cycling effects can be considered if the methodology is based on the proposition that the principal effect of fatigue loading is the reduction in material strengths due to accumulation of localized damage. In fiber matrix composites, the matrix is especially susceptible to fatigue damage, but the fibers remain largely unaffected. Due to matrix wearout, it is proposed that there is significant reduction in strength, but the composite stiffness remains unaltered. Experimental results confirm the validity of this assumption.

Processing modifications in the failure analysis to consider fatigue effects are also included in the flow chart given in figure 5. It assumes the existence of unidirectional residual strength data as a function of both the number of fatigue cycles and the load level that are used as input (fig. 6). In this case, least failure loads are calculated and compared to the applied load to determine failed elements based on degraded residual strengths. Laminate residual strength can be determined using the residual unidirectional strengths.

Unidirectional residual strength data for compression fatigue are not available. For this reason, only the damage states at various load steps are predicted for quasi-static loading. To consider effects of fatigue for correlation with experimental data, the matrix dominated strengths are reduced to a third of the static ultimate. Moduli and strength properties used in calculations are listed in table 2.

EXPERIMENTAL PROGRAM

Two sets of laminates were chosen for the study. One set was made up of fiber dominated $[0_2/\pm45]_{5s}$ and $[0/45/0/-45]_{5s}$ laminates, and the other set was quasi-isotropic $[0/\pm45/90]_{5s}$ and $[90/0/\pm45]_{5s}$ laminates fabricated from both T-300/5208 and T-300/5209 material systems.

TEST SPECIMEN DESIGN AND FABRICATION

The test specimen configuration, along with its dimensions, is shown in figure 7. The specimens were 1.0 inch wide with a 0.250 inch diameter circular hole located in the center of the unsupported span. The hole was drilled with a diamond coring bit to minimize any potential damage incurred during the process. The end tab length was 2.0 inches. To reduce the applied stress on the end tab adhesive, and thereby reduce the risk of debonding, it was desirable to increase the bonded area by increasing the end tab length. This was not possible, however, due to limitations imposed by the test fixture.

The gage length of the specimens tested in this program was 2.0 inches. In determining this dimension, the objective was to maximize the gage length without reaching a state of instability resulting in gross laminate buckling failures. The reason for maximizing the gage length was to minimize the grip effects. Specimen stability was verified experimentally under static loading, as well as with the Euler buckling calculation. One specimen of each type was strain gaged during static loading. The electrical resistance strain gages used to measure the strain in the test section and the far field strains were 0.0625 inch and 0.125 inch, respectively, and are also shown in figure 7.

Fabrication of the test specimens was performed using NARMCO T-300/5208 and T-300/5209 prepreg material. Panels with the required stacking sequences were laid up and cured in an

autoclave using a two-step cure cycle with temperatures of 250°F and 350°F and a pressure of 85-100 psi with no post curing. The panels were then examined for uniformity using ultrasonic C-scan techniques, tabbed, and cut into individual specimens with a rotary diamond saw. The end tab material was a glass-reinforced, epoxy resin material. The adhesive used to bond the end tabs to the Graphite-Epoxy specimens was Hysol Aerospace Adhesive EA 9309, which was selected due to the flexibility of its bonds, as well as its high peel strength. Each of these properties is important in fatigue tests so as to prevent debonding of the end tabs.

TEST PROCEDURE

All tests were performed with an Instron Model 1321 closed-loop, servo-hydraulic test machine. The test fixture employed in the tests was the IITRI compression fixture shown in figure 8. The existing fixture was initially designed for a maximum specimen width of 0.75 inch. For this reason, it was necessary to redesign the grips to accommodate the necessary 1.0 inch specimen width. With the new grips, it was necessary to drill a hole in the specimen end tab to allow for a connecting bolt. This hole is indicated in figure 7. The location and clearance of the hole were selected so as to have a minimal effect on the test results. Prior to each test, the IITRI fixture was aligned and the clearance checked so as to provide uniform noneccentric loading. These checks were made using a rigid specimen bolted in the grips, and a telescoping clearance gage, respectively. No lateral support mechanism was deemed necessary in view of the results of the preliminary static tests which indicated no gross buckling problem with the gage length being tested.

Fatigue tests were conducted on nine specimens of each laminate group. The test program is summarized in table 3. The specimens were subjected to sinusoidal compression-compression fatigue loadings with a frequency of 10 Hertz and R = 0.1,

S levels (maximum stress/ultimate stress = S) ranging from 0.50 to 0.75, and number of cycles (N) of 5×10^5 cycles and 1×10^6 cycles.

Of major interest during the course of the fatigue tests was the initiation and subsequent growth of the damage produced. To follow the course of events, each specimen was removed from the test machine at regular intervals of 2.5×10^5 cycles and subjected to nondestructive inspection by means of ultrasonic C-scan techniques. In order to detect any initial damage that may have occurred during fabrication, scans were made of the untested specimens. At the completion of the fatigue tests, a group of C-scans was developed from which the damage initiation and propagation could be observed. Examples of such scans are given in the next section, where they are correlated with the analytical results.

An important observation which cannot be derived from the C-scan image is the location of the delamination with respect to the laminate thickness. A method which was used to establish these data is analysis of the waveform obtained using the ultrasonic C-scan equipment and an oscilloscope. The procedure is as follows.

First, a C-scan is made of the specimen and then the transducer is located over the damaged area. The waveform on the oscilloscope will show the front surface ultrasonic echo, the back surface echo, and a delamination echo located between the two, the location of which is proportional to the location of the damaged region in the specimen thickness between the front and back surfaces. An example of this is shown in figure 9. By using the following equation, the lamina location can be derived:

$$L = \frac{D}{ID} \times N$$

where

L = Lamina number from front surface
D = Distance between front surface echo and damage echo
ID = Interface delay
N = Number of laminae.

Such an analysis yielded the location to be approximately between the first and second plies or the second and third plies, and was verified from photomicrographs of some of the specimens.

During the course of the experiments, a problem which arose was that of debonding of the end tabs from the laminate. Despite the use of high strength adhesive, fatigue life of the adhesive was not sufficient to prevent failure. The debonding was initially noticed during one of the earlier scanning intervals as a small light area underneath the end tab which started at the leading edge adjacent to the test section. Subsequent examinations at later intervals revealed further debonding and finally, in some cases, complete separation of the end tab and the specimen. An initial consideration to alleviate the problem was to increase the area of the end tab, thereby reducing the average shear stress. This was found to be impossible due to size restrictions imposed by the IITRI fixture. The solution to the problem came with the design of a set of wedge blocks to fit in the fixture at each end of the test specimen. These blocks are shown in figure 8. Their function was to support the specimen over its end area and distribute a portion of the fixture loading over this area as an axial load, thus reducing the shear stress level present in the adhesive interface. The results were very favorable with only minor debonding occurring at higher stress and cycle levels. There was also no brooming of the end fibers, which was of initial concern during the block design.

Of the three specimens of each group fatigued, one was strain gaged like the static test specimens during the residual strength testing, and one was sectioned for photomicrographic analysis.

Residual strength measurements are given in table 4.

In an effort to examine in detail the fatigue induced damage, selected specimens were sectioned and photomicrographed. Specimens were sectioned both parallel and perpendicular to the longer axis tangent to the notch (fig. 10). These areas were chosen in order to include the major damage regions. The preparation of the section began by cutting a 0.1 inch slice from the desired location on the specimen with a rotary diamond saw. The section was then mounted in Buehler Epoxide Resin and polished. The polished surface is produced by a 0.3 micron abrasive proceeding though 11 successive polishing stages. All photomicrographs in this report were taken at a magnification of 50X.

RESULTS AND CORRELATION STUDIES

Predicted damage states for all the laminate types tested are presented in this section, and a qualitative correlation is attempted. Because of lack of data on strength degradation of constituent laminae and interfaces, no quantitative comparison is made with growth of disbonds due to load cycling as observed in ultrasonic C-scans. These scans show the initiation and growth of disbonds near the top and bottom surfaces of the specimens. The disbonds which occur in between are usually masked and cannot be detected. Photomicrography after sectioning can detect all such disbonds as well as intralaminar cracking in the section. This technique can be utilized, however, only after failure occurs or loading is terminated, and therefore growth of damage cannot be monitored. Representative photomicrographs showing final states of intralaminar and interlaminar damages are also presented. Constituent properties of both resin systems used for predictions are listed in table 2. Stress states and damage states in the laminates possess a diagonal symmetry, i.e. they are unaltered after 180° rotation about the z-axis (fig. 1), and therefore damages in only half the laminate are shown.

Laminate configurations tested are of four types which are denoted as A, B, C, and D, respectively, and are described below.

A. $[0_2/\pm 45]_{5s}$

B. $[0/45/0/-45]_{5s}$

C. $[0/90/\pm 45]_{5s}$

D. $[90/0/\pm 45]_{5s}$.

Specimens of these laminates were tested statically to establish initial static strength. Other identical specimens were subjected to fatigue loading followed by residual strength evaluation. Certain of the test samples were sectioned after fatigue loading to conduct photomicrographic studies.

Since consideration of the detailed stacking sequence will make a finite element stress analysis too expensive, analyses were performed for the following configurations.

1. $[0_2/\pm 45]_s$ to model type A laminates
2. $[0/45/0/-45]_s$ to model type B laminates
3. $[0/90/\pm 45]_s$ to model type C laminates
4. $[90/0/\pm 45]_s$ to model type D laminates.

Since most of the damages are usually concentrated near the surfaces, the modeling employed for analysis seems adequate. Correlations attempted appear to confirm this adequacy.

FIBER DOMINATED LAMINATES, TYPES A AND B

Damage predictions for laminates made of both resin systems as well as the experimental observations are presented in figures 11-26. A study of these figures reveals the following characteristics.

Effect of Resin Systems

Predicted damage states for both resin systems (figs. 11,12, 14,15) are similar. Elastic moduli of the two systems are nearly equal, but there are differences in strengths in the virgin state as well as those assumed for degraded states. However, it appears that these differences are not enough to produce any significant change in predicted damage states. The C-scans (figs. 16, 17) and ply damages observed in the photomicrographs also do not

show any significant differences in damage propagation characteristics. Therefore, changing the matrix material from 5208 to 5209 does not affect the damage states, but noticeable differences are oabserved in residual strengths (table 4). Similar changes may be expected in lifetime. As mentioned earlier, no attempt is made in this study for calculation of residual strength or lifetime and therefore no experimental/analytical correlation is made for these characteristics.

Damage Patterns in Type A Laminates

The quasi-static analysis predicts delamination to initiate from the notch at the 0/+45 interface at an angle of $\pm 60°$ to the load direction. Growth of delamination at the 0/45 interface with increase of load obtained from a five step analysis is shown in figure 13. Although growth of delamination under quasi-static loading and fatigue could be different in nature, some similarities are noticeable in the initial stages of quasi-static loading and initiation of damage due to fatigue. Similarities are also seen in the predicted final damage states and those observed at the end of load cycling (see figs. 11-17). Delaminations at the end of quasi-static loading appear to have grown somewhat in the load direction, but primarily across the width of the notch (figs. 12,13,15). Some delaminations are also predicted at the ± 45 interface (figs. 12,15), which also have grown in the load direction (0°) across the width of the notch.

Extensive intraply damages, which are due to matrix failure, are predicted (figs. 11,14) in all the laminae. The failure criterion predicts failure due to the combined effects of transverse and shear stresses and therefore no distinction is made between transverse failure and shear disbonding. Matrix failure in the 0° plies is predicted to grow in the load direction, but restricted to the width of the notch. 45° ply damages, however, appear to have extended in two directions, along the fibers as well as in the direction perpendicular to them, initiating at notch edges at 45° to the load direction.

Delamination damage in both resin systems can be observed in the C-scans (figs. 16,17). The delamination initiates on both sides of the notch (at 0/45 interface near the surface) at the axial tangent points and propagates towards the end tabs. The regions of delamination initially develop in all four quadrants around the notch in a uniform and symmetric manner. Growth of each region then progresses along the axial tangent line to the notch as well as along the circumference of the notch towards the center of the specimen. This circumferential progression eventually results in the bridging of the delamination in the upper two quadrants and, similarly, in the lower two quadrants. Upon completion of the joining of these regions, the delamination continues towards the end tabs, contained within a region bounded by the axial tangent lines to the notch (figs. 16,17). This behavior is similar to what is predicted for quasi-static loading, which of course considers strength degradation due to fatigue, although in a relatively crude fashion. The delamination predicted at the ±45 interface is not detected in the C-scans. Photomicrography of the failed specimens facilitates a very close examination of the matrix microcracking within the plies as well as the interlaminar damage not detected in the ultrasonic C-scans.

Photomicrographs of the axial and transverse sections of specimen 8-A-4 show damage typical to this laminate stacking sequence. Figure 18 shows an axial section tangent to the circular notch. Looking at the ultrasonic C-scans (figs. 16,17), it becomes evident that this section contains a damage zone along the right side of the hole. Visual inspection of the photomicrograph reveals numerous intralaminar microcracks occurring in the +45° and -45° plies. Close examination shows that practically in all cases the cracks appear to have either initiated at or terminated at the 0° ply interface. It is also observed that where the crack tip meets a 0° lamina interface, there exists very frequently a matrix rich region. The presence of these regions provides a possible site for initiating the microcracking, i.e. they act as stress concentrations along the interface and

serve as crack initiators during the fatigue process. The distribution of cracks is relatively random, and in most cases the crack distribution is directed perpendicular to the 0° fiber direction.

A section of specimen 8-A-4 which is a cut in a transverse direction tangent to the notch is shown in figure 19. Aside from a small number of randomly distributed cracks, the majority of cracks are shown to be oriented collinearly and confined essentially to the 0° plies. The cracks extend completely through each group of two 0° plies and terminate at the angle ply interfaces. It should be noted that all of the cracks in the collinear orientation are aligned with the cracks in the 0° plies on the surfaces, which are observed to originate at the edge of the hole on the C-scan (figs. 16,17). The only obvious delamination is found at the 0/+45 interface nearest to the surface as noted earlier. This indicates that while the delamination is limited mainly to the surface layers, as indicated on the C-scans, the axial crack propagation shown on the surface 0° plies also extended in a similar fashion through each set of 0° plies throughout the thickness.

Damage Patterns in Type B Laminates

Changing the stacking sequence by introducing the 45° ply between the two 0° plies results in significant differences in the damage patterns. The in-plane damage predicted is somewhat less than that in $[0_2/\pm45]_s$ laminates, and the interlaminar damage, though present at all the interfaces, is significantly reduced (figs. 20-23). The greatest extent of delamination is predicted to occur at the 0/-45 interface, and it appears to have grown around the notch in the load direction. The C-scans in figures 24 and 25 also show that the delamination damage is limited at the notch edges. Compared to the delaminations found in the C-scans for the type A laminates, the type B layup has negligible interlaminar damage, and can be expected to have better fatigue characteristics.

A photomicrograph of specimen 9-B-8 is presented in figure 26 and is typical of this stacking sequence. There is much less microcracking and interlaminar damage as seen in the transverse section. The 0° plies do not have the collinear axial splitting type of crack propagation extending through the entire thickness like those observed in the type A laminates. The section shows that there is little delamination in the laminate, and that it occurs at the 0/-45 interface and the 0/45 interface similar to the quasi-static predictions. The greatest amount of microcracking is observed near the surfaces tangent to the diameter of the notch. There is a little crack propagation in the 0° plies, but it extends through the 45° plies. Residual strength data (table 4) show that this is the only stacking sequence which yields residual strength higher than the static ultimate. The change in the stacking sequence, therefore, reduces the delamination damage as well as microcracking and appears to improve the fatigue response and residual strength.

QUASI-ISOTROPIC LAMINATES, TYPES C AND D

To broaden the study on the effect of the matrix and the stacking sequence on the laminate response to compression fatigue, a quasi-isotropic laminate configuration has also been analyzed and tested. Damage growth predictions for two stacking sequences of quasi-isotropic laminates of both resin systems are presented in figures 27-42.

Effect of Resin Systems

In these laminate configurations, the C-scans of the test specimen show damage initiating and growing in approximately the same regions for the two resin systems. This is also true for the intraply matrix damage observed in photomicrographs. The analysis also shows that the differences in the properties of the 5208 and 5209 matrix systems are not significant enough to affect

the location of damage initiation and growth, as in the case of fiber dominated laminates. The change in the matrix, however, affects the residual strengths and, to some extent, the rate of damage growth.

Damage Patterns in Type C Laminates

The FLAC model predicts in-plane matrix failures principally in the ±45° plies, with very little damage in the 0° or the 90° plies (figs. 27,30). There are few failures in the 90° ply because the transverse compressive strength is much greater than the transverse tensile strength. The 90° ply takes up a substantial part of the transverse load, reducing the transverse tensile stress in the 0° ply. Therefore, there are no splitting type of cracks transverse to the load in the 0° ply similar to those found in the type A laminates. The location of the failures predicted in the 45° plies, however, is similar, occurring around the ±45° lines to the load direction initiating at the notch edge and extending along the fibers and transverse to them. These damages appear to grow across the width of the laminate. The principal delamination is predicted to occur at the 0/45 interface, and extend to the sides (figs. 28,29,31) as compared to the strong 0° orientation in the type A laminate. Experimental results confirm that delamination does occur at the 0/45 interface near the surfaces and tends to grow around the notch edges transverse to the load, as can be seen in figures 32 and 33. Some amount of delamination is also predicted to occur at the ±45 interface and this, too, does not have the tendency to grow in the load direction as observed in the type A laminates. Little delamination is predicted to occur at the -45/90 interface.

Both the in-plane and the interlaminar damages can be studied from the photomicrographs of the failed specimens. Damage in specimen 8-C-14 is typical and the transverse section is shown in figure 34. This section shows little microcracking in the laminate, but clearly shows the delaminations at the 0/45 and at the

±45 interfaces near the surfaces, with the surface 0° ply having buckles and failed.

Other photomicrographs show some cracking in the ±45° plies. The overall damage pattern for this stacking sequence, as predicted, fairly correlates with the damages experimentally found.

Damage Patterns in Type D Laminates

Changing the stacking sequence to $[90/0/\pm45]_s$ appears to have little effect on the damages which are predicted and observed in contrast to changes in the fiber dominated laminates. The overall damage pattern in the plies of the type D laminate (figs. 35,38) is similar to that predicted for the type C layup (figs. 27,30). The delamination damage predicted is also similar, as can be seen from figures 28, 29, 31, 37, and 39. The experimental results also seems to confirm this, as seen in the C-scans (figs. 40,41). Photomicrographs of failed specimens (fig. 42) show little in ply damage, though microcracking in the ±45° plies is observed in some specimens. The axial section of specimen 9-D-11 shows delaminations at the 0/45 and the ±45 interfaces, but little microcracking. The major delamination is not near the surface ply but is located at the 0/45 interface near the surface, as in the case of type C laminates, although some delaminations are observed by the C-scans which appear to be at the 90/0 interface.

FAILURE MECHANISMS

In this subsection the failure mechanisms are critically examined for four laminates of Graphite/Epoxy (T-300/5208 and T-300/5209) which have been tested. Since the two resin systems have different maximum process temperatures (350°F for 5208 and 250°F for 5209) it can be expected that resin controlled failure mechanisms may be different for the two systems. However, the static failure mechanisms for the two materials' systems appear

to be identical. Damage patterns generated during fatigue also do not change much due to the change in resin systems, although some differences do exist in the rate of damage growth and residual strength, as pointed out earlier. Failure mechanisms and damage growth due to fatigue, however, are strongly influenced by laminate stacking sequence. In what follows, an attempt is made to obtain an understanding of this phenomenon.

Type A Laminates

The influence of fatigue loading upon failure modes, as observed in residual strength tests, is most pronounced for laminate type A. Two distinct failure modes are observed for laminates of types A and B. They are the diagonal shear (DS) failure and the net compression (NC) failure modes which are illustrated in figure 43. Fatigue damage in the type A laminate appears to be manifested as cracking of the +45° and -45° laminae in regions adjacent to the central notch. In regions where the +45° laminae are cracked, the -45° laminae are not, and in regions where the -45° laminae are cracked, the +45° laminae are not damaged, as illustrated in figure 44. As can be seen, the -45° laminae exhibit cracking in the first and third quadrants, while the +45° laminae are cracked in the second and fourth quadrants. The origin of the fatigue cracking in the ±45° laminae can be attributed to the shearing stresses which act tangent to the circular notch and parallel to the load direction. The distribution of the shearing stress in this region is an antisymmetric function, as shown in figure 45. The direction of the shearing stress can be determined by a free body diagram as shown in figure 46. Acting at the remote end of the free body is the constant, applied stress $\bar{\sigma}$, while at the section adjacent to the hole, the compressive stress varies from $K_T^{\infty}\,\bar{\sigma}$ at the edge of the hole to $\bar{\sigma}$ at some distance from the hole. Since the two resultant forces are not equal, a third force is required for equilibrium. The third force is the resultant of the shearing

stresses and its direction is the same as the remote applied stress, since the resultant force at the section adjacent to the hole will always be greater than the resultant of the remote stress. Hence, when the shearing stress is transformed to a coordinate system rotated 45° from the axis of the specimen, transverse tensile stresses act on the -45° laminae and transverse compressive stresses act on the +45° laminae in the first and third quadrants. This behavior is reversed in the second and fourth quadrants as shown in figure 47.

One significant observation of the residual strength failure of type A laminates is that the diagonal shear failure appears to be primarily responsible for laminate failure, although the net compression failure mode is also present. Further, the diagonal shear failure mode is always found to occur parallel to the +45° laminae. No -45° diagonal shear failures are observed. Since the +45° laminae in type A laminates are located nearest to the surface, it is likely that cracks in these laminae, which are developed during fatigue cycling, play a role in the ultimate failure mode.

Another mechanism observed in type A laminates is growth of cracks due to fatigue in the 0° laminae parallel to the load direction and tangent to the edge of the circular notch (fig. 19). The cracks are noticeable in all 0° laminae with their surfaces contained in a single plane tangent to the notch where axial sections were taken for photomicrography (see fig. 10). The delaminations which are generated at the intersection of the axial cracks and the near-surface 0/45 interface can be seen to grow monotonically with increasing cycles or stress amplitude, as observed in the C-scans. This delamination, however, is not primarily responsible for the ultimate failure of the laminate. The most likely sequence of events leading to the final failure appears to be the shear failure of the 45° ply below the surface plies which then become unsupported and buckle. Buckling of the large delaminated portion just above the notch does not occur, since it is not transferring load in direct compression. (Failures of notched and unnotched specimens are shown in figs. 48,49.)

Type B Laminates

Type B laminates are similar to those of type A. They also exhibit characteristics of the diagonal shear and the net compression failure modes. Diagonal shear appears to be the predominant mode of failure with net compression appearing in a small number of instances. In contrast to type A laminates, the shearing direction in type B specimens is not always parallel to the near-surface angle ply (+45°). Failures are found to occur in the -45° direction as well as in the +45° direction. A third distinct diagonal shear failure which is observed is the "dual shear" failure, in which the shear failure is in the +45° direction on one side of the notch and in the -45° direction on the other side of the notch, as illustrated in figure 50.

A study of these failures indicates a connection between the direction of failure and the delaminations noticed after failure. It should be emphasized that no significantly large delamination is noticed in the C-scans after fatigue cycling is stopped and residual strength tests are performed. In all instances the delaminations are such that subgroups of 0° plies with an angle ply "sandwiched" in between are formed. Two cases are noticeable. The first case (I) is that in which the subgroups have a configuration of [0/+45/0]. In this case, the direction of shear failure is that of the +45° lamina. The subgroups of the second case (II) have a [0/-45/0] configuration resulting in a -45° shear direction. Dual shear failure appears to take place when both types of delamination are present, with case I on one side of the notch and case II on the other side. A similar effect is present in the type A laminate in which the 0/+45 interfaces below the areas nearest to the surface appear to remain intact, resulting in a +45° shear direction.

A further observation pertaining to the diagonal shear failure mode is that the origin of the crack appears to be at the boundary at 45° to the load direction, as shown in figure 51. Also, microscopic analysis of laminate type B shows that

while intralaminar cracking of the angle plies is present as in type A, it occurs to a lesser degree because of the difference in stacking sequence. Despite this, however, the cracking of the angle plies and its subsequent relation to the diagonal shear failure mode observed in laminate type B is consistent with the previous explanation of this failure mode in type A.

The net compression failure mode is noticeable along with the diagonal shear failure mode in a small number of specimens tested. In those instances, it is generally confined to the near-surface layers with the shear failure extending through most of the specimen thickness. The net compression failures are characterized by delamination between the angle plies and the 0° plies, leaving individual 0° plies unsupported and prone to local instability. This is in contrast to the subgrouping of the 0° plies and the angle plies in the diagonal shear mode. Between the zones of diagonal shear and net compression failures are large interlaminar cracks which extend past the damage zone parallel to the loading direction as well as from edge to edge in the transverse direction.

The overall failure sequence in laminate type B appears to be that fatigue induced damages in the angle plies caused out-of-plane deformation as well as delamination of the laminate into subgroups. This induces bending stresses which cause kinking of the 0° plies parallel to the cracks in the "sandwiched" angle ply, with the direction being determined by that of the angle ply. Net compression sometimes follows the shear failure, due to unsymmetric loading which results after the shear failure.

Quasi-Isotropic Laminates - Types C and D

The quasi-isotropic laminates exhibit failure mechanisms common to both stacking sequences. The predominant failure mode is that of net compression with the fracture line running transverse to the load direction directly through the center of the

notch (figs. 52,53). Extensive interlaminar disbonding is observed extending past the damage zone parallel to the load direction across the width of the test specimens. In most cases the delaminations occur at the 0/45 interface. Photomicrographic observations reveal very little cracking within the individual laminae, unlike the extensive cracking noticed in the type A laminates. The 90° plies not only take up most of the transverse load, but along with the 0° plies, reduce the shear load on the laminate.

In the type C layup, residual strength failures show delaminations at the 0/45 interface near the surface as well as at the ±45 interface. The probable sequence of events leading to ultimate failure is delaminations created at the 0/45 interface nearest to the surfaces due to fatigue loading (in the load bearing parts) causing the 0° surface ply to become unsupported. Buckling then occurs in this 0° ply and leads to a catastrophic failure. This is unlike the failure in the type A laminate, where the surface 0° plies become unsupported primarily due to shear failures in the 45° ply.

The type D layup also shows similar mechanisms. The fatigue loading induces delamination at the 0/45 interface near the surface. This results in the surface 90/0 plies becoming unsupported. The surface 90° ply contributes little to the stability of the 0° ply. When the 0/45 delamination grows over a certain area (if it is not already of sufficient dimensions), it creates buckling instability in the 0° ply. Such failures are also observed during load cycling.

The principal failure mechanism involved in the failure of both quasi-isotropic laminates in compression fatigue, therefore, is the growth of delaminations near the surface plies, which causes local instability of the 0° ply leading to its buckling. The subsequent propagation of failure occurs almost simultaneously and consists of delaminations between the plies or groups of plies, as observed in fiber dominated laminates. This can be seen very clearly from the photomicrograph of the axial section of laminate 9-D-11, where the surface 90/0 plies have

deformed out of plane followed by delaminations of the 45°, -45°, 90°, 0°, and the +45° plies.

RESIDUAL STRENGTH

Since the principal assumption in the present analysis is the degradation of the matrix in fatigue, residual strengths of the laminates with the two matrix systems have been measured after subjecting them to fatigue loading. Of the three specimens in each group, two have been tested for residual strength and the third has been sectioned for photomicrography. The results of these tests are presented in table 4. With only two specimens per group, the test results may not be representative of the exact behavior. Quantitative comparisons, however, are made for some general observations.

Average residual strengths as a percentage of the static strength are presented in table 4 for different fatigue loadings. In both stacking sequences of the quasi-isotropic layup, fatigue induced damages are seen to cause reductions in residual strength by varying degrees, and cycling at 0.6 σ_u is seen to cause failures before the end of load cycling. At this level all the type C specimens with the 5209 matrix have failed. In the type D laminates, however, all specimens with the 5208 matrix have failed, and while one of the 5209 specimens shows a residual strength of 87% of the static value, the other specimen tested has failed in fatigue. In the fiber dominated laminates, while some strength reduction is observed in the type A stacking sequence, significant increase in strength is observed for the type B stacking sequence for both matrix systems. This is the only set of laminates where an increase in noticed. There has been only one fatigue failure in the type A stacking sequence. This has occurred in the 5209 resin system, but the other specimens show residual strengths of about 94% of the static ultimate.

From these limited data, it may be concluded that the 5209 matrix system appears to degrade more rapidly than the 5208 matrix. The 5208 matrix system seems to be more resistant to fatigue induced damage. Dispersing the laminae like that in type B (in contrast to type A) appears to improve the fatigue characteristics of fiber dominated laminates. Further tests appear necessary, however, before final conclusions are drawn.

BUCKLING ANALYSIS

The critical failure mechanisms were identified in a previous subsection and it can be concluded from the discussions that separation of surface plies either due to delaminations or due to failure of plies just below those on the surface results in buckling of the separated ply or ply groups. To obtain a better understanding of this mechanism, a buckling analysis has been performed. Buckling is structurally governed; hence buckling of surface plies depends on the size and shape of the delamination as well as the laminate layup. In this study, only a few sample problems are considered for studying buckling of 0° plies. No attempt is made to develop a failure criterion. Understanding the failure mechanism using a simplified model and an elastic buckling analysis is the only objective.

The delaminated ply is modeled as an orthotropic plate with different boundary conditions. The finite element code ANSYS is used to perform the buckling analysis. ANSYS uses a displacement formulation, first calculating the static stress solution and then solving the buckling eigenvalue problem to obtain the buckling loads and the corresponding mode shapes. For the purpose of ascertaining the accuracy of the finite element model, closed form analytical solutions and series of solutions for buckling loads of isotropic and orthotropic plates with different boundary conditions have been compared to the finite element predictions. Experimental results show that the delaminated ply or plies may possibly be approximated as three types of plates with boundary conditions as shown in figure 54.

For the type I plate the width is fixed at 0.24 inch, approximately the notch diameter, and the length, chosen as the characteristic dimension, is varied. For the type II and type III plates, an aspect ratio of 1.5 is chosen and the length, chosen as the characteristic dimension, is varied between 0.24 and 0.48 inch, approximately between one and two notch diameters.

These dimensions are realistic, as can be seen from the C-scans of various specimens. The buckling loads calculated can therefore be compared with load levels applied on the test specimens. The critical load predicted by ANSYS is a stress resultant acting on the ply. It is necessary to translate this ply load into an average load on the laminate. This load varies from laminate to laminate, and can be easily calculated using lamination theory. Since the delaminated ply may have some matrix damage in it, a netting analysis is also used to relate the ply and the laminate load and can be used as a bound.

The delaminated 0° ply for type C laminates, as observed in the C-scans, can be modeled either as the type II plate or as the type III plate. The finite element buckling analysis has been conducted using a mesh of 36 rectangular plate elements. The critical buckling loads for the 0° ply are calculated for characteristic lengths of 0.24, 0.36, and 0.48 inch. These are plotted in the form of a stress on the 0° ply against the characteristic length, and are presented in figure 55. As seen from table 5, these convert to different average stresses for different laminates. For the type C and type A laminates, these stresses for a netting analysis and a lamination theory analysis are presented in table 6. At a characteristic length of 0.36 inch, with clamped boundary conditions on all sides of the plate, the laminate stress predicted to cause buckling varies between 37.9 ksi for the elastic case and 32 ksi for the netting analysis.

An increase of the characteristic length to 0.42 inch reduces the buckling loads to 32 ksi and 28 ksi, respectively. Stresses for type II plates are also shown in table 6. With a

static net section strength (notched) of 62 ksi, and fatigue cycling at stresses greater than 0.5 σ_u, the cyclic load is sufficient to create instability in the plate for both sets of boundary conditions. Delamination regions yielding characteristic lengths of these magnitudes are possible, as can be seen from the experimental results plotted in figure 56. This simplified ply buckling model, together with the experimental characteristic lengths, shows the buckling loads to be of the same magnitude as the applied fatigue load. For this reason a good number of the quasi-isotropic specimens have been observed to fail during fatigue loading. On the other hand, results obtained for the type I plate (fig. 54) show the buckling loads to be excessively high and therefore delaminations of that type observed in fiber dominated laminates are not the cause of buckling failure. As has been observed in residual strength tests, buckling of parts like the type II plates usually occurs in fiber dominated laminates after failure of ±45° plies causes the surface plies to become unsupported. This phenomenon has been discussed in a previous subsection. The approach used here (in its present form) can by no means be used as a criterion to predict failure due to buckling of surface plies, but it demonstrates analytically the possibility of such failures, especially in quasi-isotropic laminates.

This limited analysis, together with experimental observations, however, shows that although propagation of delamination is the primary mechanism leading to final ply buckling type failure in quasi-isotropic laminates, this does not appear to be the case in fiber dominated laminates. Therefore, the delamination propagation model utilized in reference 4 should be used with some caution and growth of intralaminar damages should be considered for prediction of failure in fiber dominated laminates.

CONCLUSIONS

Failure mechanisms for notched composite laminates subjected to compression fatigue are complex and dependent upon laminae stacking sequences and properties. Different laminates showed different failure modes in the exploratory tests conducted herein and preliminary analyses suggest the reasons for this.

The test program was conducted on a series of laminates using a test specimen which attained the expected static strength levels in its unnotched configuration. Notched static strength showed reasonable effects of hole stress concentrations, although no correlation with analysis was attempted.

Cyclic loading introduced various damage mechanisms, changes in residual strength, and fatigue failure which were carefully documented experimentally and examined analytically. The principal results may be summarized as follows:

1. Fiber dominated laminates and quasi-isotropic laminates show different patterns of damage growth under fatigue. For fiber dominated laminates, dispersing the layers in the layup like the one used in $[0/+45/0/-45]_{5s}$, as compared to grouping them together as in $[0_2/\pm 45]_{5s}$, can make a laminate more damage tolerant.
2. Growth of interlaminar as well as intralaminar damages occurs in all types of laminates. Interlaminar damage growth leads to final failure due to buckling of surface plies in quasi-isotropic laminates; while in fiber dominated laminates, intralaminar damage in the angle plies are usually severe and lead to final failure.
3. Changing the resin system from 5208 to 5209 does not have any significant influence on the damage patterns, but may have some effect on residual strength and/or lifetime. Data are too limited to confirm this. Additional tests are required using resin systems which have more significant differences than those of 5208 and 5209.

4. An iterative technique using finite element stress analysis together with appropriate failure criteria for intralaminar and interlaminar damage can be utilized to predict damage propagation around the hole due to quasi-static and fatigue loading. For fatigue, consideration of local residual strength degradation is necessary, and comprehensive test programs to generate data on such degradation in unnotched coupons are essential for better analytical predictions.

REFERENCES

1. Hahn, H. T., "Fatigue Behavior and Life Prediction of Composite Laminates," in ASTM STP 674, 1979, p. 383.

2. Staff, C. R., "Compression Fatigue Life Prediction Methodology for Composite Structures - Literature Survey," NADC-78203-60, Warminster, Pa., June 1980.

3. Badaliance, R., and Din, H. D., "Compression Fatigue Life Prediction Methodology for Composite Structures, Vol. II," Technical Proposal, McDonnell Aircraft Company, Report No. MDAC 5723, February 1979, as referred to in reference 2.

4. Ratwani, M. M., and Kan, H. P., "Compression Fatigue Analysis of Fiber Composites," NADC-78049-60, Warminster, Pa., September 1979.

5. McLaughlin, P. V., Jr., Kulkarni, S. V., Huang, S. N., and Rosen, B. W., "Fatigue of Notched Fiber Composite Laminates, Part I: Analytical Model," NASA CR-132947, March 1975.

6. Ramkumar, R. L., Kulkarni, S. V., and Pipes, R. B., "Evaluation and Expansion of an Analytical Model for Fatigue of Notched Composite Laminates," NASA CR-145308, March 1976.

7. Kanninen, M. F., Rybicki, E. F., and Griffith, W. I., "Preliminary Development of a Fundamental Analysis Model for Crack Growth in a Fiber Reinforced Composite Material," ASTM STP 617, p. 53.

8. Humphreys, E. A., and Rosen, B. W., "Development of a Realistic Stress Analysis for Fatigue Analysis of Notched Composite Laminates," NASA CR-159119, March 1979.

9. Pipes, R. B., and Pagano, N. J., "Interlaminar Stresses in Composite Laminates under Uniform Axial Extension," Journal of Composite Materials, October 1970.

10. Roderick, G. L., NASA-Langley Research Center, private communication.

Table 1. Failure Criteria

Tensile Fiber Mode

$$\sigma_{11} = \sigma_A^+$$

Compressive Fiber Mode

$$\sigma_{11} = -\sigma_A^-$$

Tensile Matrix Mode

$$\frac{1}{\sigma_T^{+2}} \sigma_{22}^2 + \frac{1}{\tau^2} \sigma_{12}^2 = 1$$

Compressive Matrix Mode

$$\frac{1}{\sigma_T^-} \left[\left(\frac{\sigma_T^-}{2\tau} \right)^2 - 1 \right] \sigma_{22} + \frac{1}{4\tau^2} \sigma_{22}^2 + \frac{1}{\tau^2} \sigma_{12}^2 = 1$$

Tensile Interlaminar Mode

$$\frac{1}{\sigma_T^{+2}} \sigma_{33}^2 + \frac{1}{\tau^2} (\sigma_{13}^2 + \sigma_{23}^2) = 1$$

Compressive Interlaminar Mode

$$\frac{1}{\sigma_T^-} \left[\left(\frac{\sigma_T^-}{2\tau} \right)^2 - 1 \right] \sigma_{33} + \frac{1}{4\tau^2} \sigma_{33}^2 + \frac{1}{\tau^2} (\sigma_{13}^2 + \sigma_{23}^2) = 1$$

Table 1 (Continued). Failure Criteria

where

σ_A^+ = axial tensile strength

σ_A^- = axial compressive strength

σ_T^+ = transverse tensile strength

σ_T^- = transverse compressive strength

τ = shear strength

Table 2. Lamina Properties Used for Calculation

Moduli	T-300/5208	T-300/5209
E_{11}	20.2 msi	19.6 msi
E_{22}	1.76 msi	1.58 msi
G_{12}	0.754 msi	0.684 msi
ν_{12}	0.38	0.38
σ_A^+	211.0 ksi	210.0 ksi
σ_A^-	204.0 ksi	204.0 ksi
σ_T^+	2.033 ksi	2.0 ksi
σ_T^-	7.133 ksi	6.94 ksi
τ (Intralaminar)	3.267 ksi	3.0 ksi
τ (Interlaminar)	2.00 ksi	1.85 ksi

Table 3. Test Program

Laminate	Matrix	Number of Specimens	Load Level (of σ_u)	Number of Cycles
$[0_2/\pm45]_{5s}$	5208	3	Static	
		3	0.5	10^6
		3	0.6	0.5×10^6
		3	0.6	10^6
$[0/45/0/-45]_{5s}$	5208	3	Static	
		3	0.5	10^6
		3	0.6	0.5×10^6
		3	0.6	10^6
$[0/\pm45/90]_{5s}$		3	Static	
		3	0.5	10^6
		3	0.75	0.5×10^6
		3	0.6	10^6
$[90/0/\pm45]_{5s}$		3	Static	
		3	0.5	10^6
		3	0.6	0.5×10^6
		3	0.6	10^6

Table 3 (Continued). Test Program

Laminate	Matrix	Number of Specimens	Load Level (of σ_u)	Number of Cycles
$[0_2/\pm45]_{5s}$	5209	3	Static	
		3	0.5	10^6
		3	0.6	0.5×10^6
		3	0.6	10^6
$[0/45/0/-45]_{5s}$	5209	3	Static	
		3	0.5	10^6
		3	0.6	0.5×10^6
		3	0.6	10^6
$[0/\pm45/90]_{5s}$	5209	3	Static	
		3	0.5	10^6
		3	0.6	0.5×10^6
		3	0.6	10^6
$[90/0/\pm45]_{5s}$	5209	3	Static	
		3	0.5	10^6
		3	0.6	0.5×10^6
		3	0.6	10^6

Table 4. Residual Strength Test Results

Laminate	Matrix	Load Level (of σ_u)	No. of Cycles	Residual Strength psi (MPa)	Strength Retention (%)
$[0_2/\pm45]_{5s}$	5208	0.5	10^6	53,975 (372.16)	87
		0.6	0.5×10^6	57,055 (393.4)	92
		0.6	10^6	54,955 (378.9)	89
$[0/45/0/-45]_{5s}$	5208	0.5	10^6	61,823 (426.27)	108
		0.6	0.5×10^6	67,432 (464.94)	118
		0.6	10^6	64,807 (446.84)	113
$[0/\pm45/90]_{5s}$	5208	0.5	10^6	44,795 (308.86)	100
		0.75	0.5×10^6	Failure	-
		0.6	10^6	41,478 (285.00)	92
$[90/0/\pm45]_{5s}$	5208	0.5	10^6	39,214 (270.38)	100
		0.6	0.5×10^6	Failure	-
		0.6	10^6	Failure	-

Table 4 (Continued). Residual Strength Test Results

Laminate	Matrix	Load Level (of σ_u)	No. of Cycles	Residual Strength psi (MPa)	Strength Retention (%)
$[0_2/\pm45]_{5s}$	5209	0.5	10^6	61,796 (426.1)	98
		0.6	0.5×10^6	63,520 (437.97)	101
		0.6	10^6	59,024 (406.97)	94
$[0/45/0/-45]_{5s}$	5209	0.5	10^6	58,768 (405.21)	100
		0.6	0.5×10^6	63,089 (435.00)	108
		0.6	10^6	63,280 (436.32)	108
$[0/\pm45/90]_{5s}$	5209	0.5	10^6	44,350 (305.79)	94
		0.6	0.5×10^6	Failure	-
		0.6	10^6	Failure	-
$[90/0/\pm45]_{5s}$	5209	0.5	10^6	45,558 (314.12)	99
		0.6	0.5×10^6	41,196	90
		0.6	10^6	Failure	87

Table 5. Lamina - Laminate Stresses

Average Laminate Stress $\bar{\sigma}_x = 1$

Laminate	Stress in 0° Ply	
	Elastic	Netting
$[0_2/\pm 45]_{5s}$	1.71	2
$[0/\pm 45/90]_{5s}$	2.53	3

Table 6. Load on $[0/\pm45/90]_{5s}$ for Buckling of 0° Ply

CHARACTERISTIC LENGTH	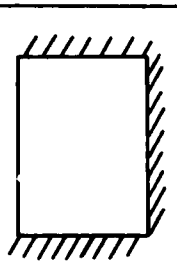 ELASTIC	NETTING	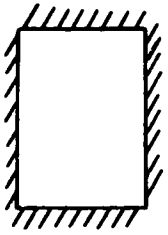 ELASTIC	NETTING
0.36	24.1	20.3	37.9	32
0.42	18.16	15.3	32.4	27.6
0.48	13.42	11.3	22.9	19.3

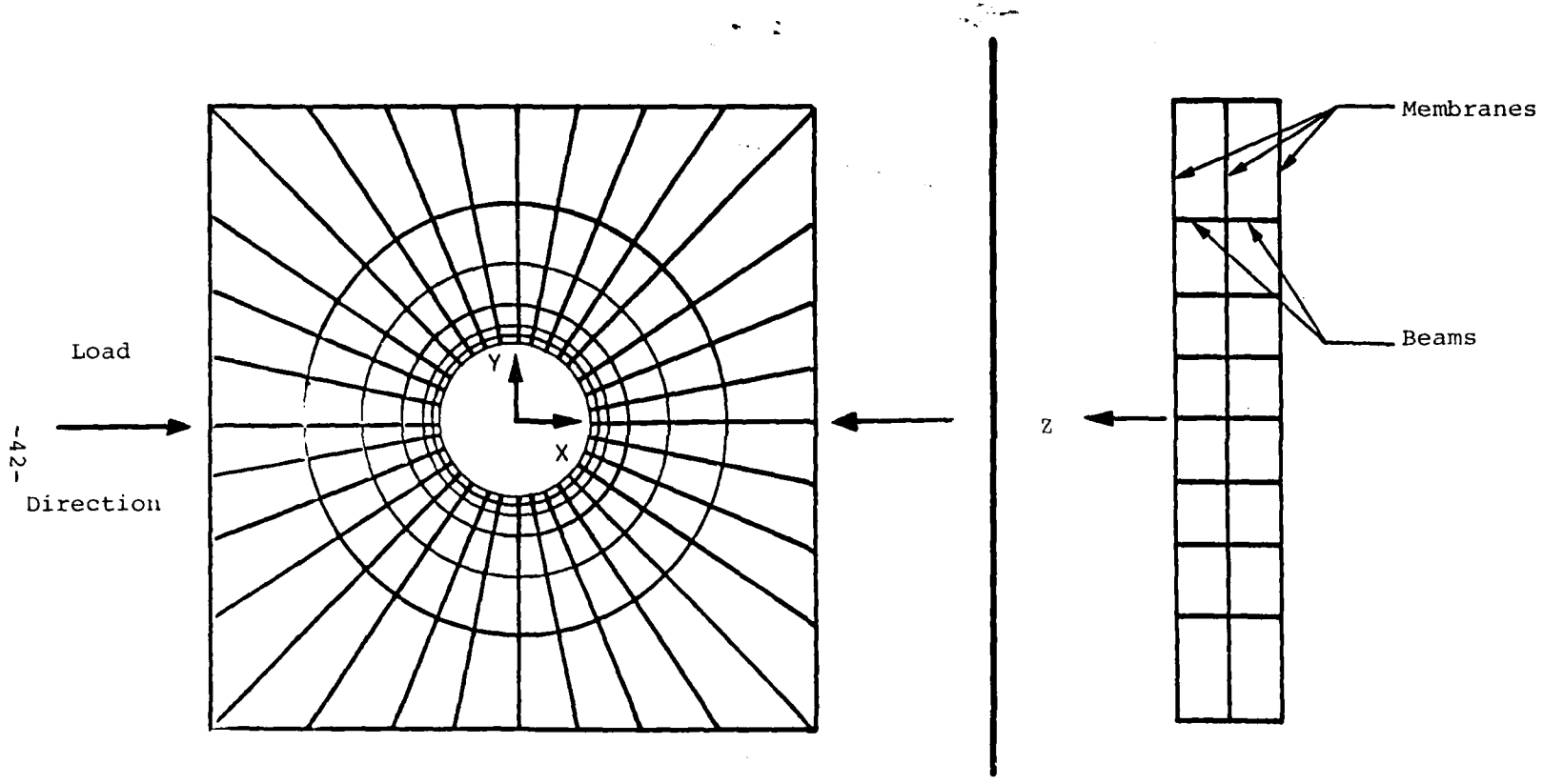

Figure 1. Beams and Membranes, Finite Element Model, Notched Plate

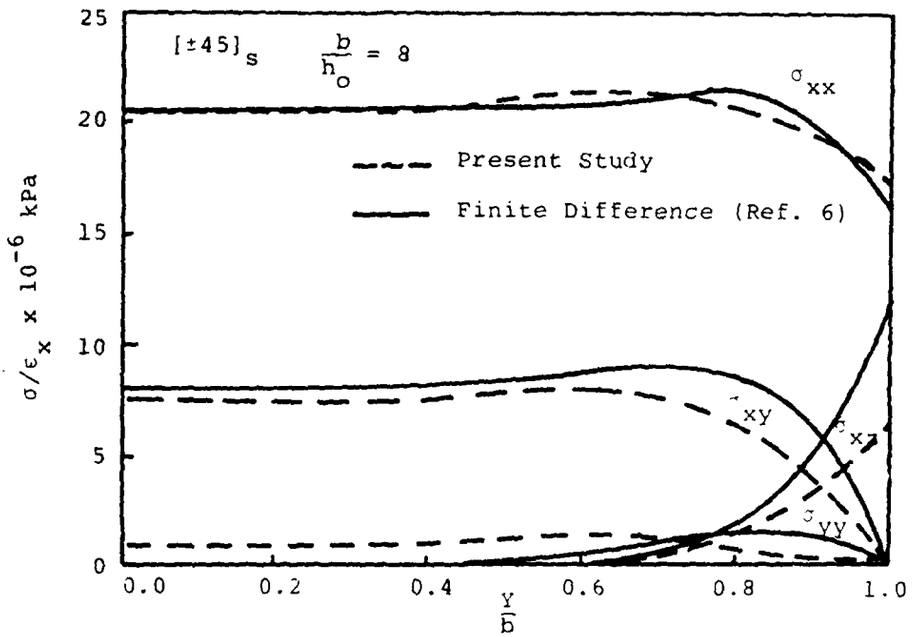

Figure 2. Comparison of Present Solution with Finite Difference Solution for $[\pm 45]_s$ Edge Effect Problem (From ref. 8)

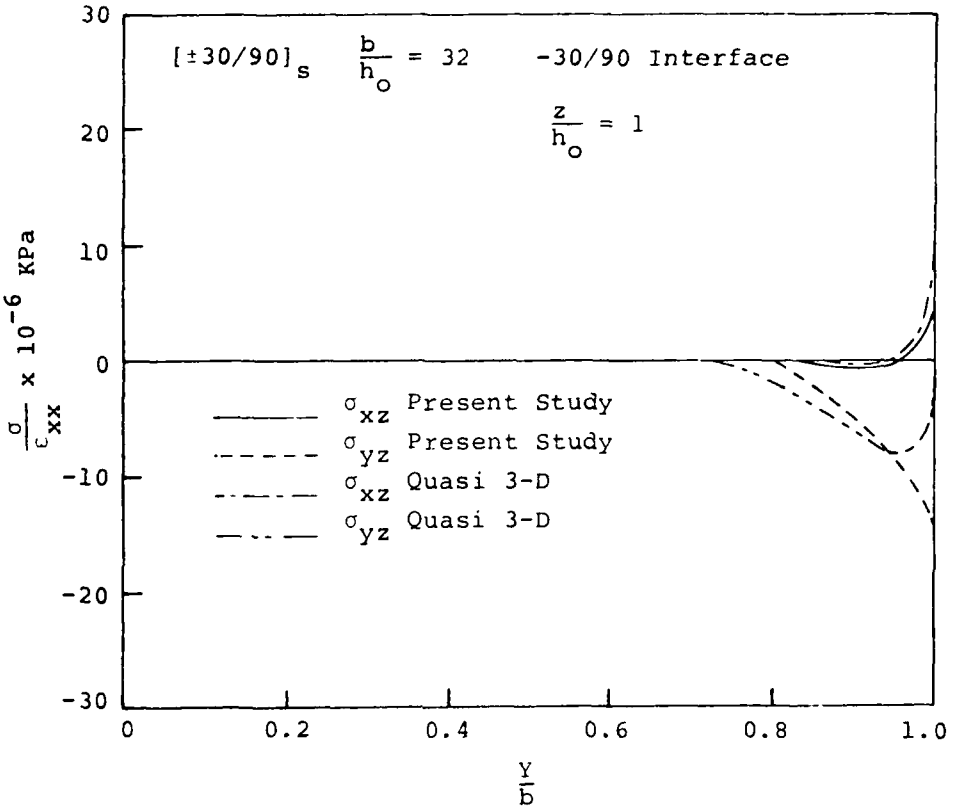

Figure 3. Comparison of Present Solution with Quasi 3-D Solution for Interlaminar Shear Stresses at $z/h_o=1$, in a $[\pm 30/90]_s$ Edge Effect Problem (From ref. 8)

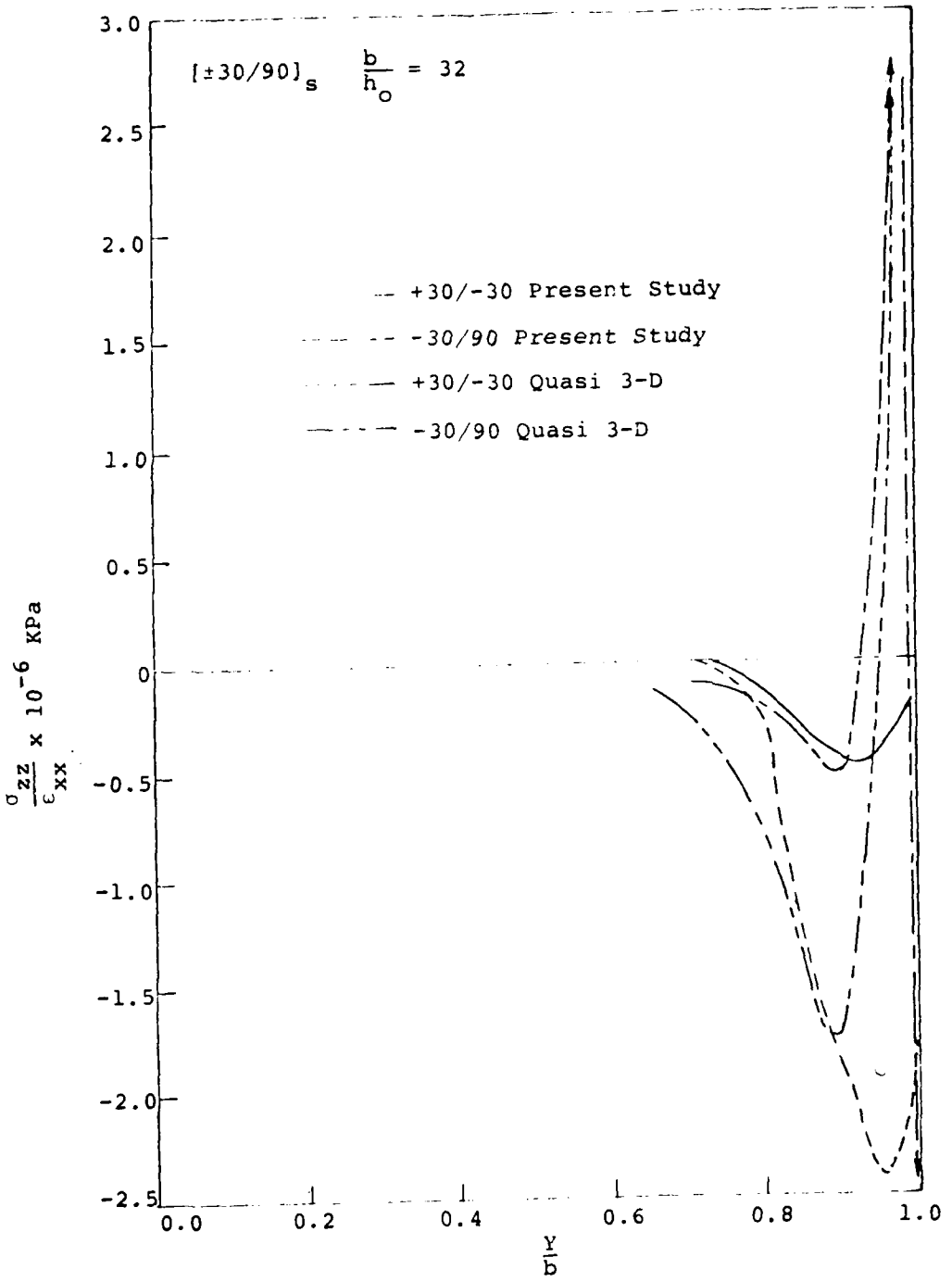

Figure 4. Comparison of Present Solution with Quasi 3-D Solution for Interlaminar Normal Stresses in a $[\pm 30/90]_s$ Edge Effect Problem

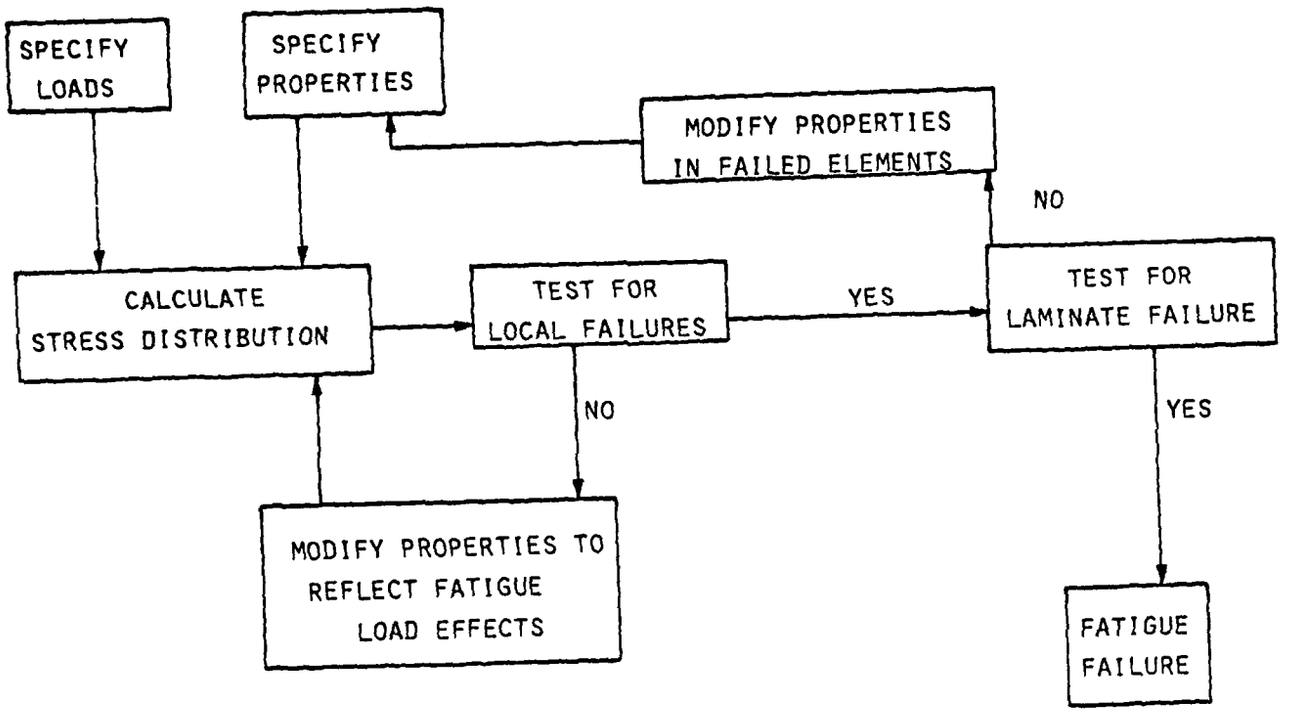

Figure 5. Methodology for Failure Analysis with Consideration of Load Cycling Effects

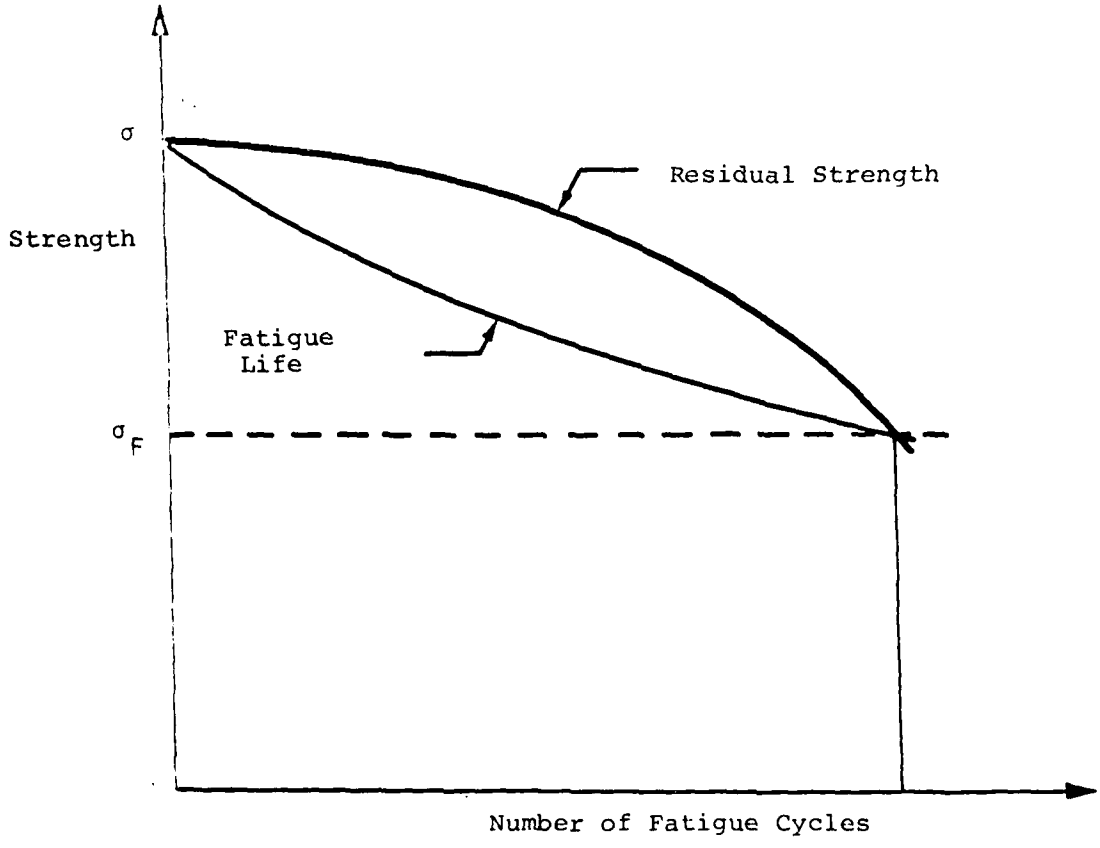

Figure 6. Residual Strength Curve of Notched Composite

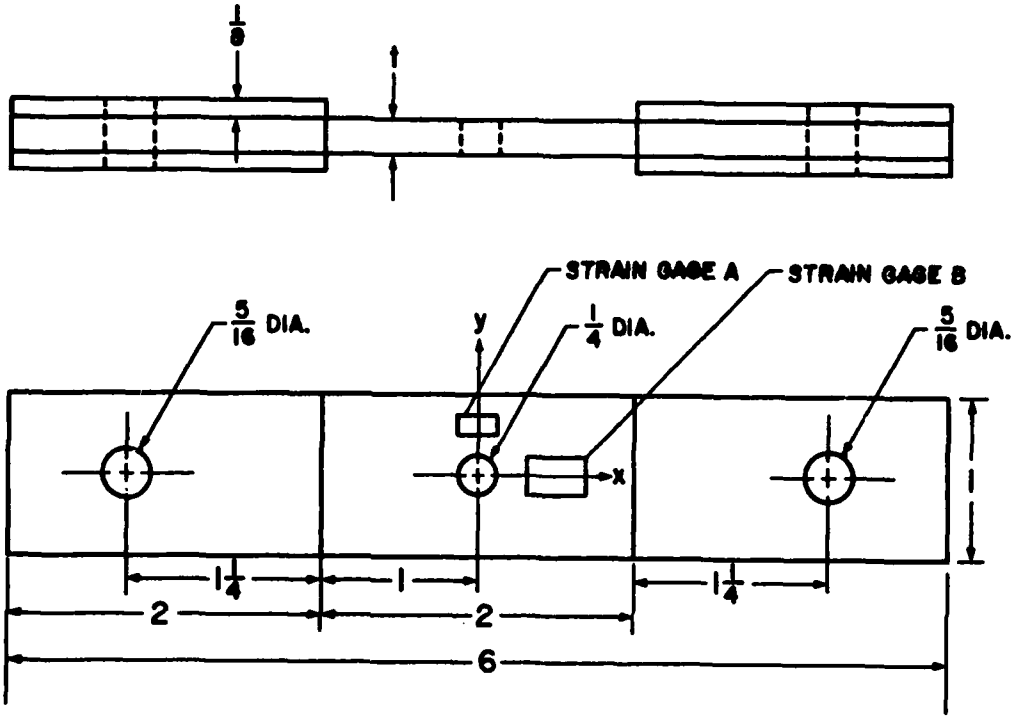

MICRO-MEASUREMENTS

STRAIN GAGE A: EA-05-125BZ-350
STRAIN GAGE B: EA-06-125AC-350

Figure 7. Notched Fatigue Specimen

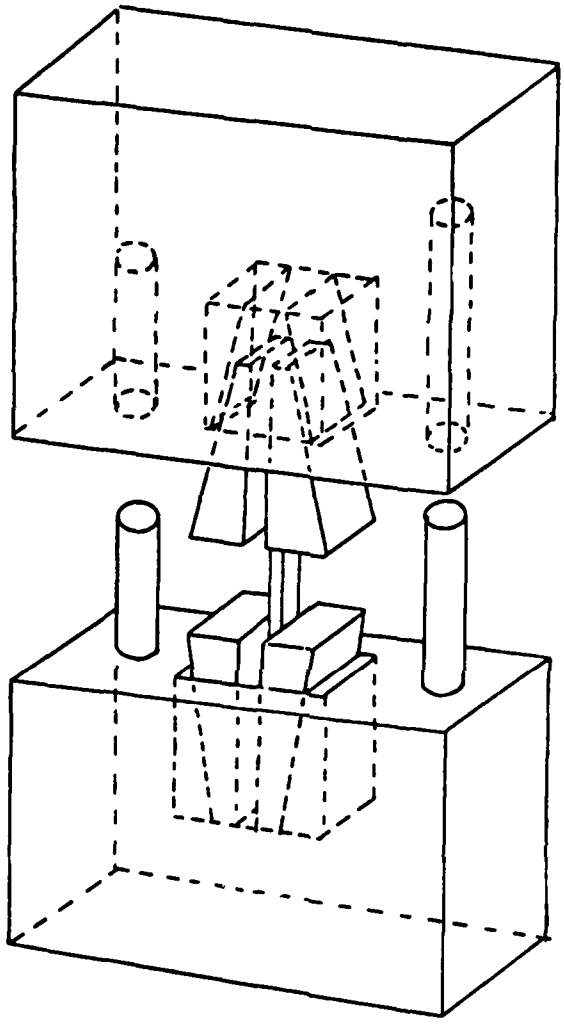

Figure 8. Modified IITRI Compression Fixture

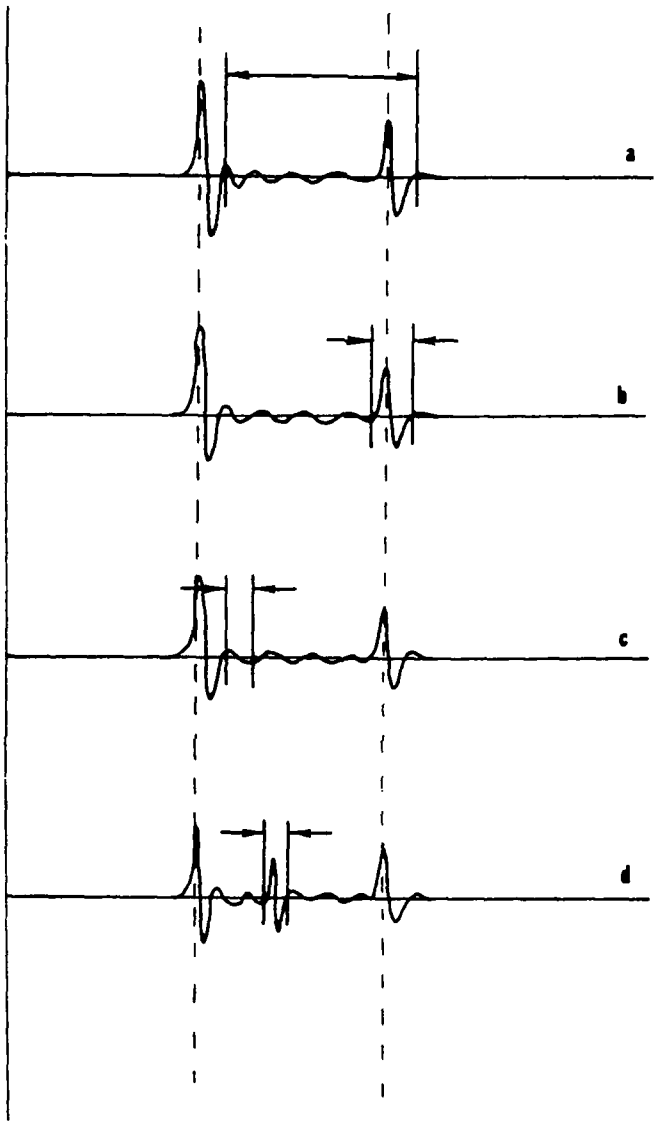

Figure 9. Gating Techniques

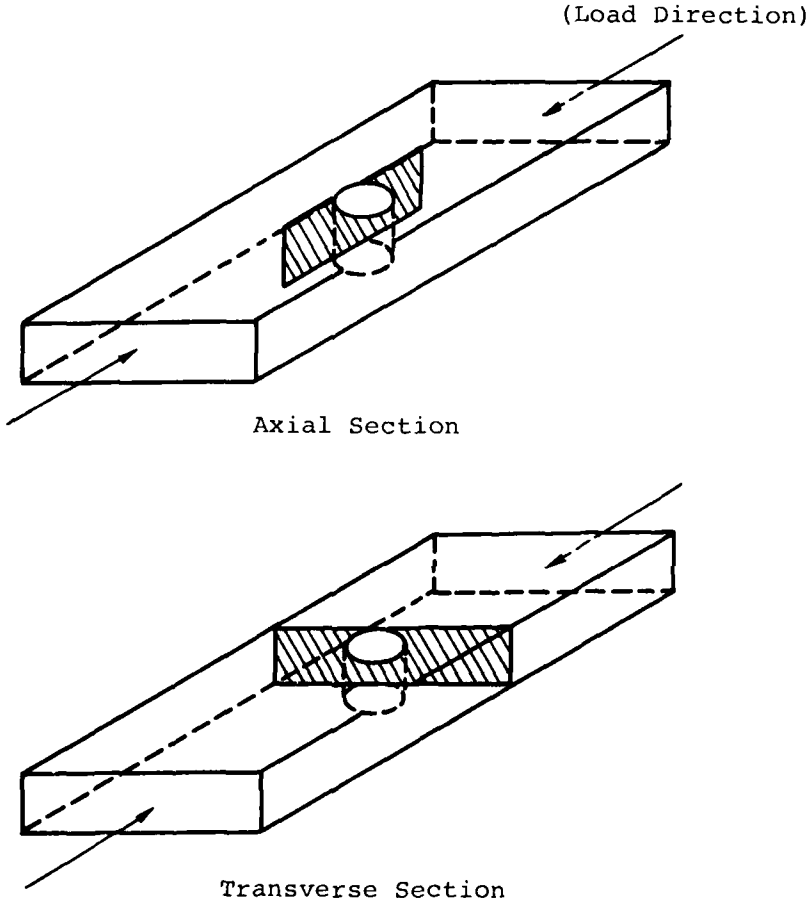

Figure 10. Micrograph Section Orientations

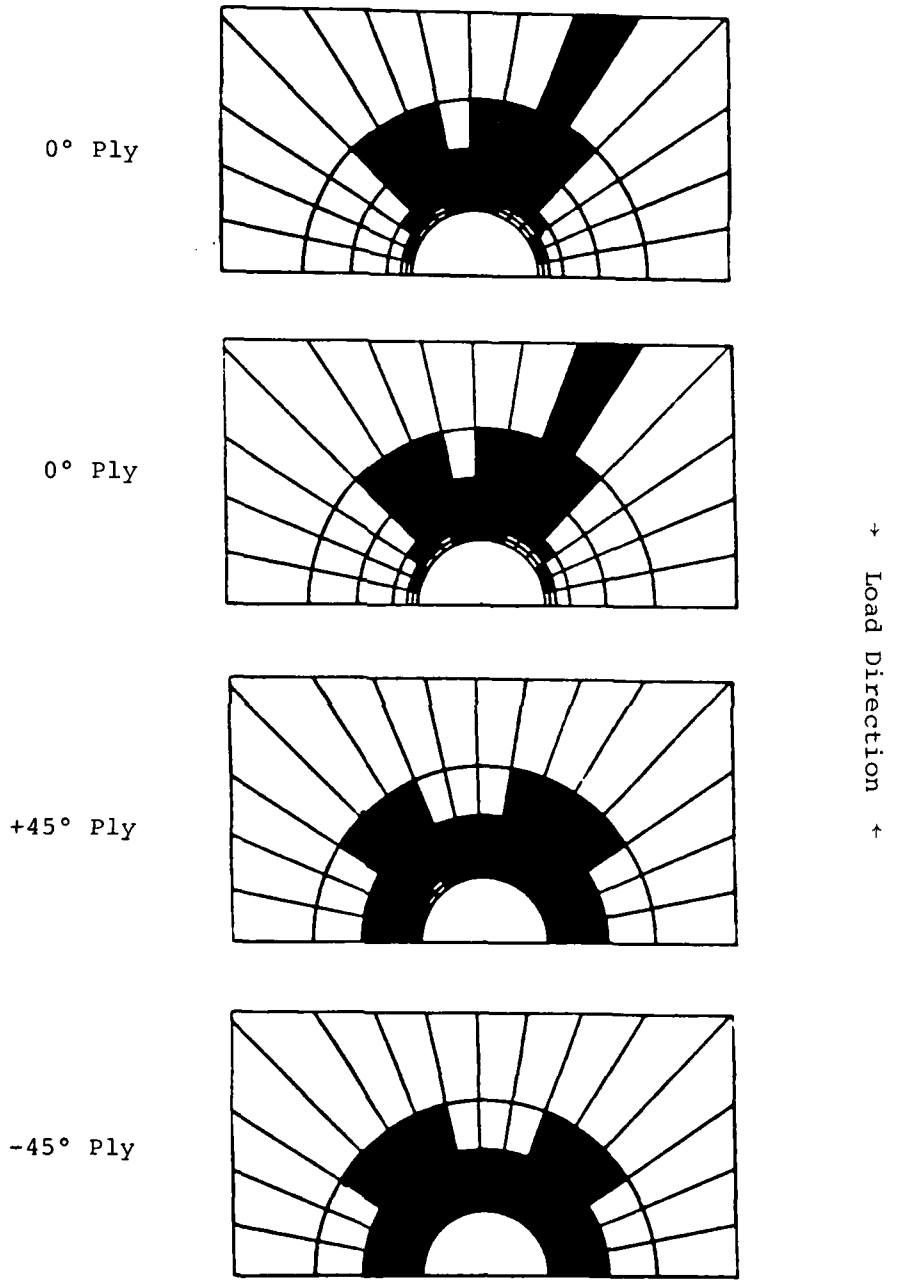

Figure 11. Intralaminar Damage in $[0_2/\pm45]_s$ - 5208 for a Load of 43.8 ksi

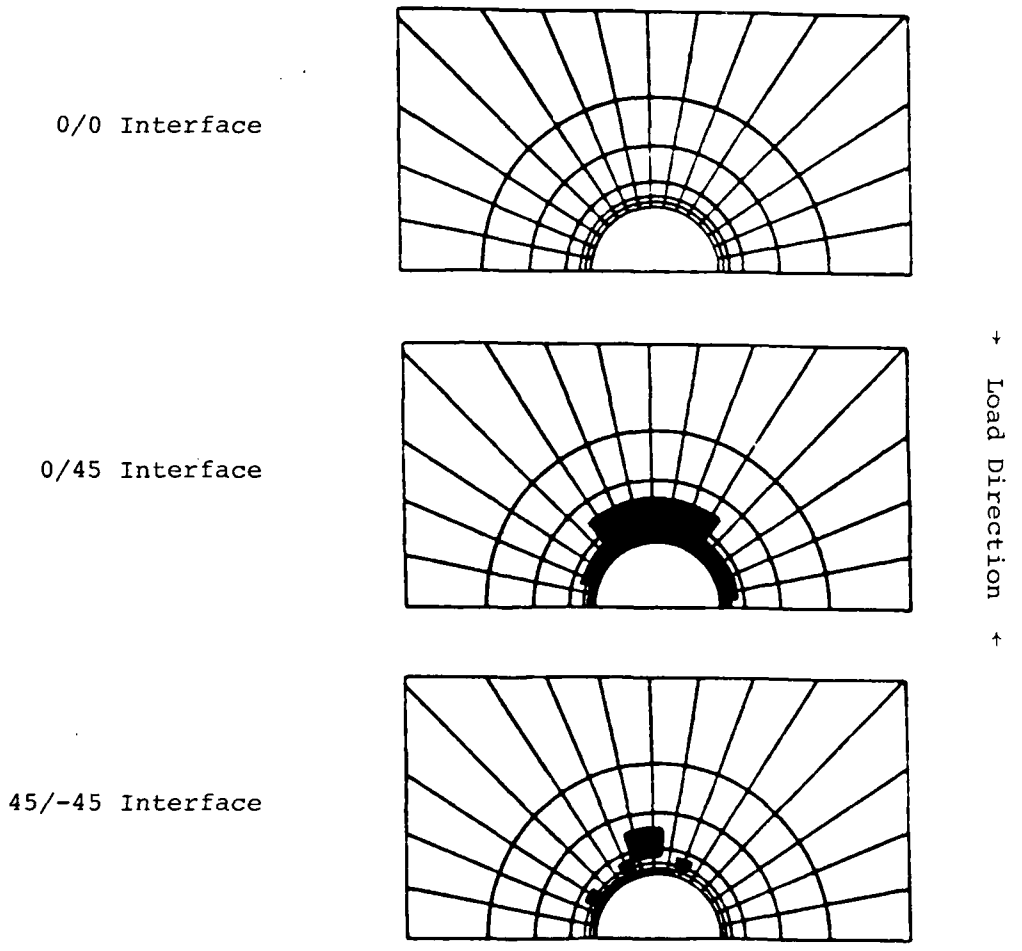

Figure 12. Interlaminar Damage in $[0_2/\pm 45]_s$ - 5208 for a Load of 43.8 ksi

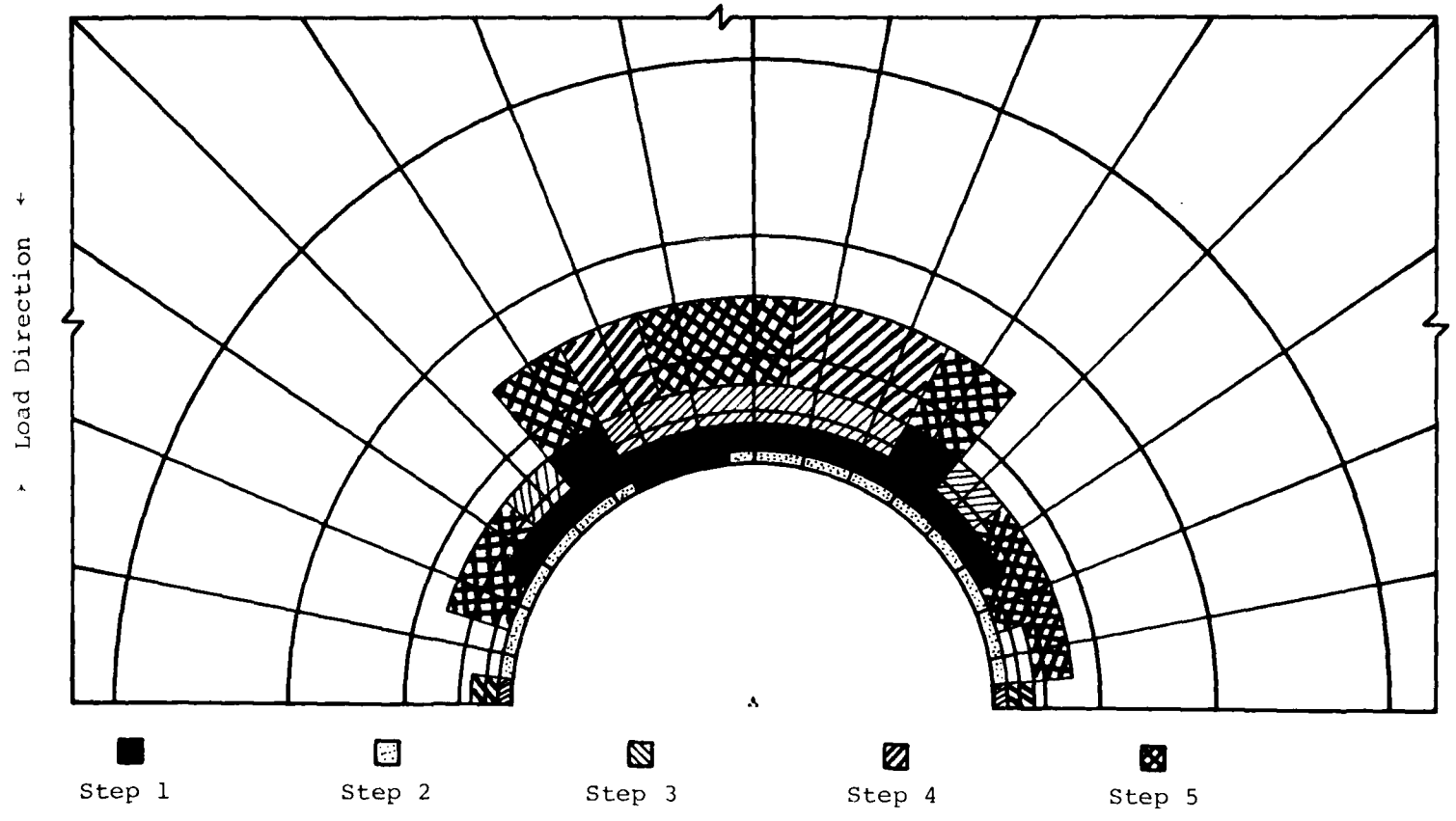

Figure 13. Interlaminar Damage Growth in $[0_2/\pm 45]_s$ - 5208 for a Five Step Analysis, Final Load of 43.8 ksi

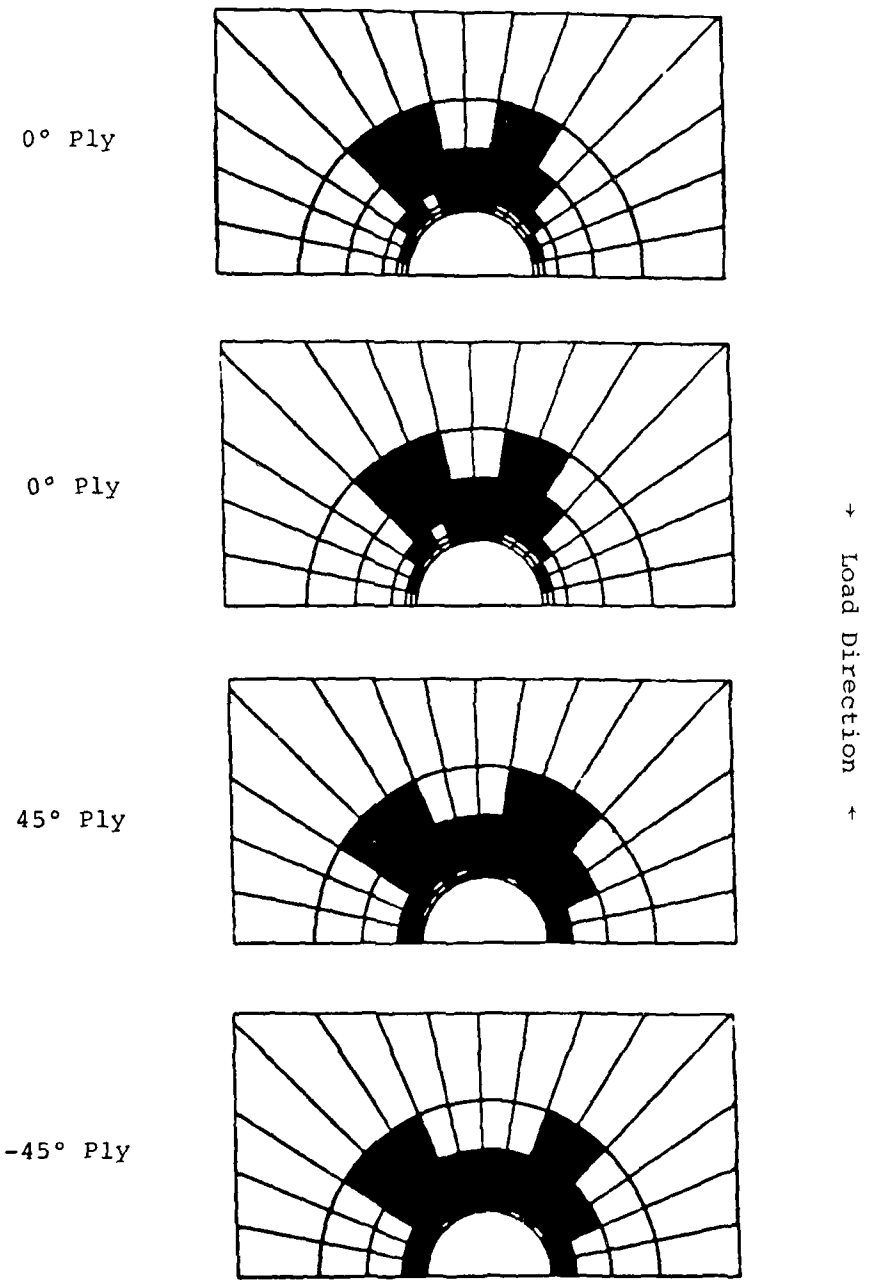

Figure 14. Intralaminar Damage in $[0_2/\pm 45]_s$ - 5209 for a Load of 39.5 ksi

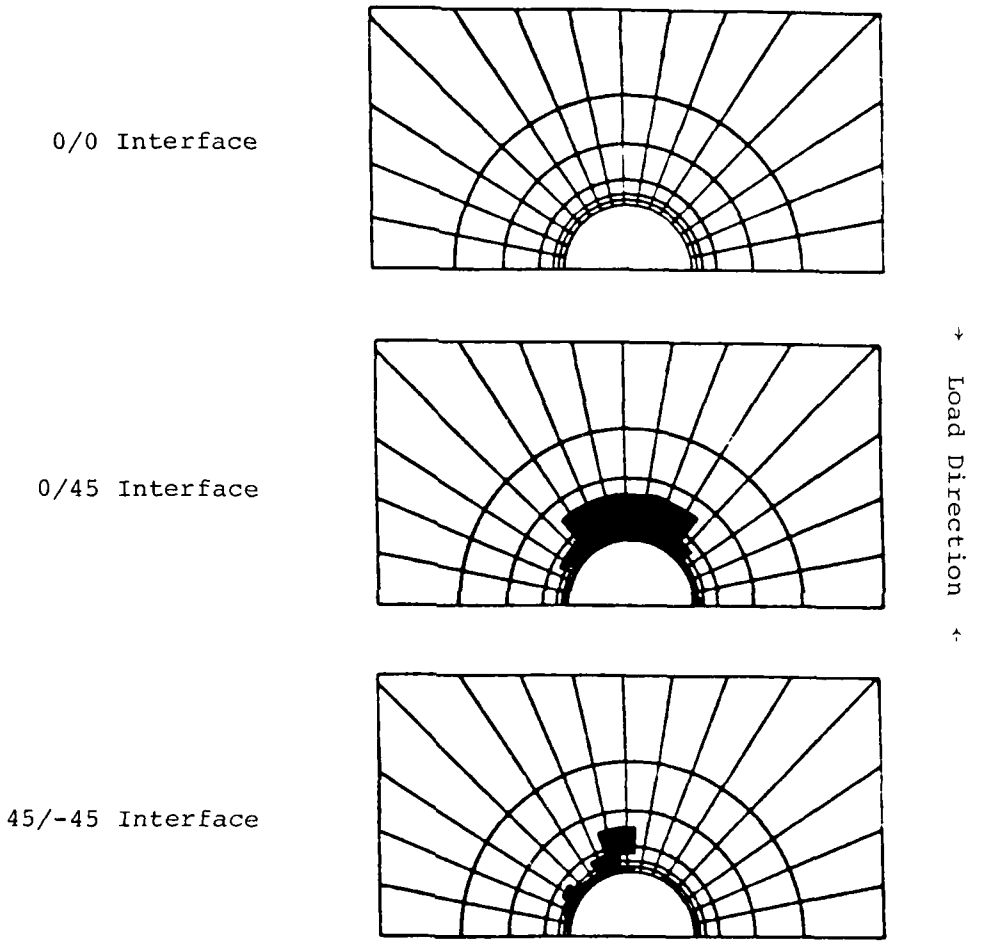

Figure 15. Interlaminar Damage in $[0_2/\pm 45]_s$ - 5209 for a Load of 39.5 ksi

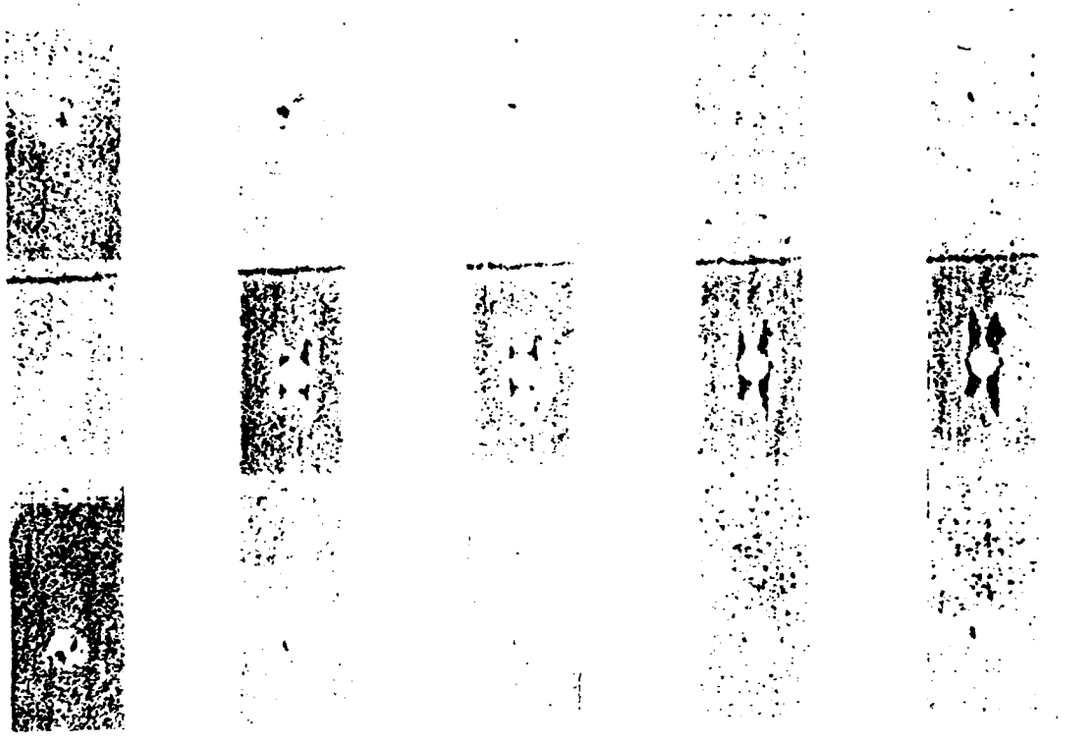

Figure 16. C-scans of Specimen 8-A-8 $[0_2/\pm45]_{5s}$ - 5208 at Different Load Cycle Levels

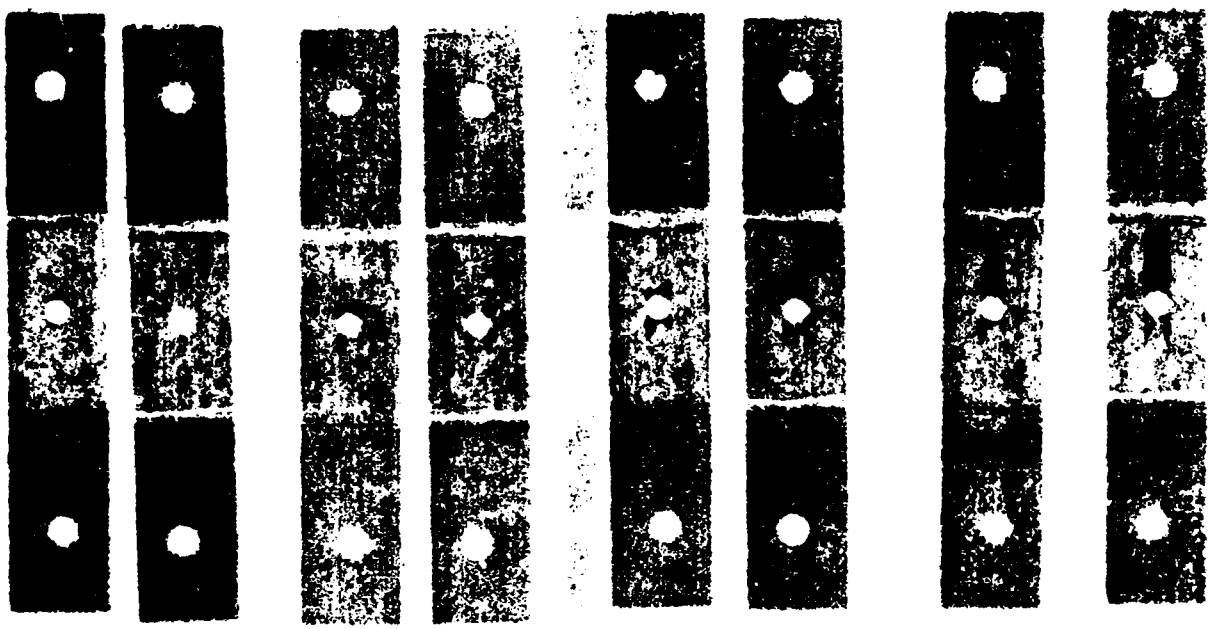

Figure 17. C-scans of Specimen 9-A-6 $[0_2/\pm45]_{5S}$ - 5209 at Different Load Cycle Levels

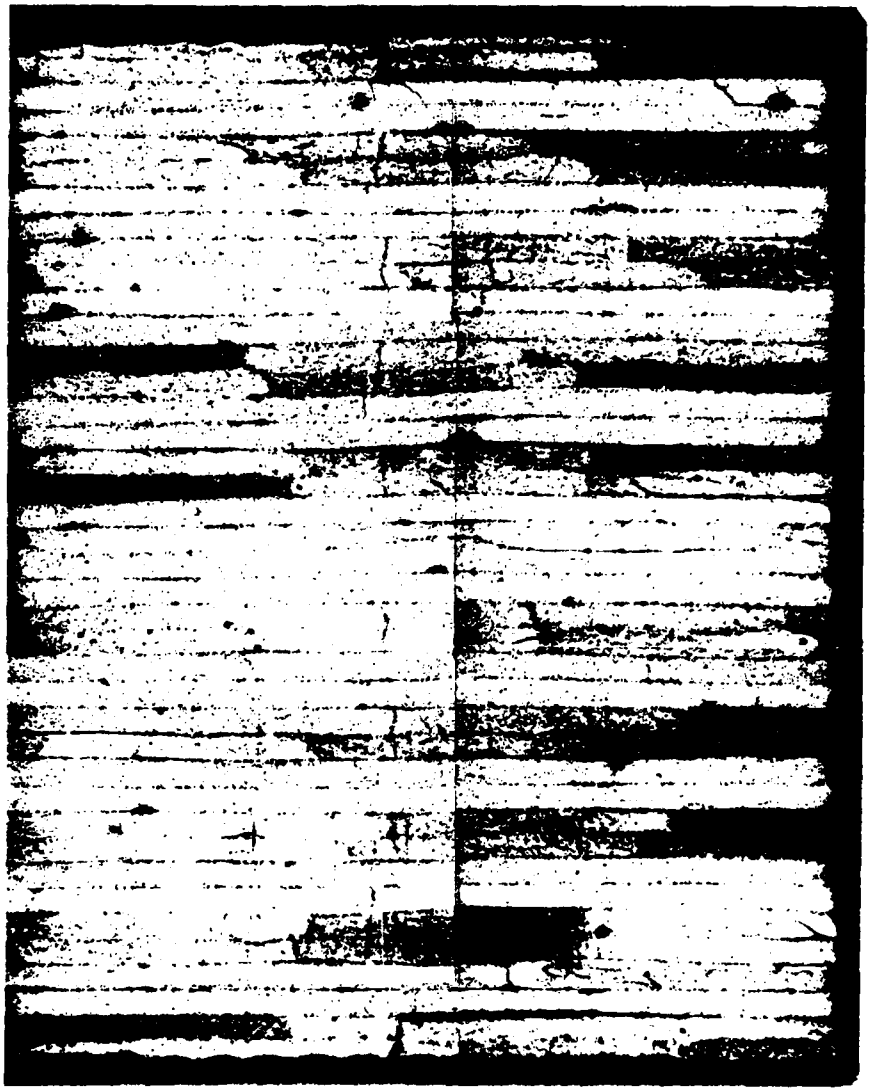

Figure 18. Transverse Section of Specimen 8-A-6 $[0_2/\pm 45]_{5s}$ - 5208

Figure 19. Axial Section of Specimen 8-A-4 $[0_2/\pm45]_{5s}$ - 5208

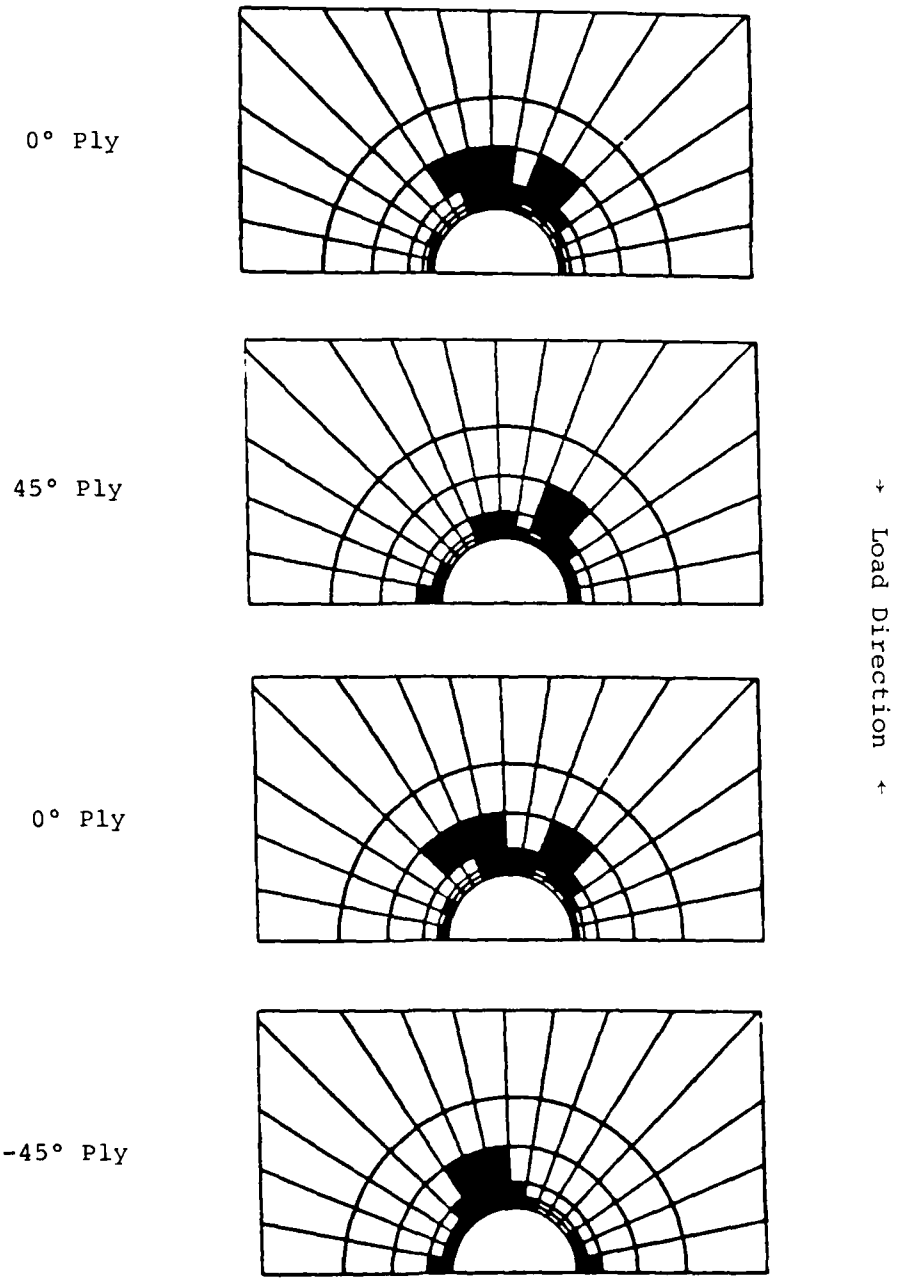

Figure 20. Intralaminar Damage in $[0/45/0/-45]_s$ - 5209 for a Load of 31.9 ksi

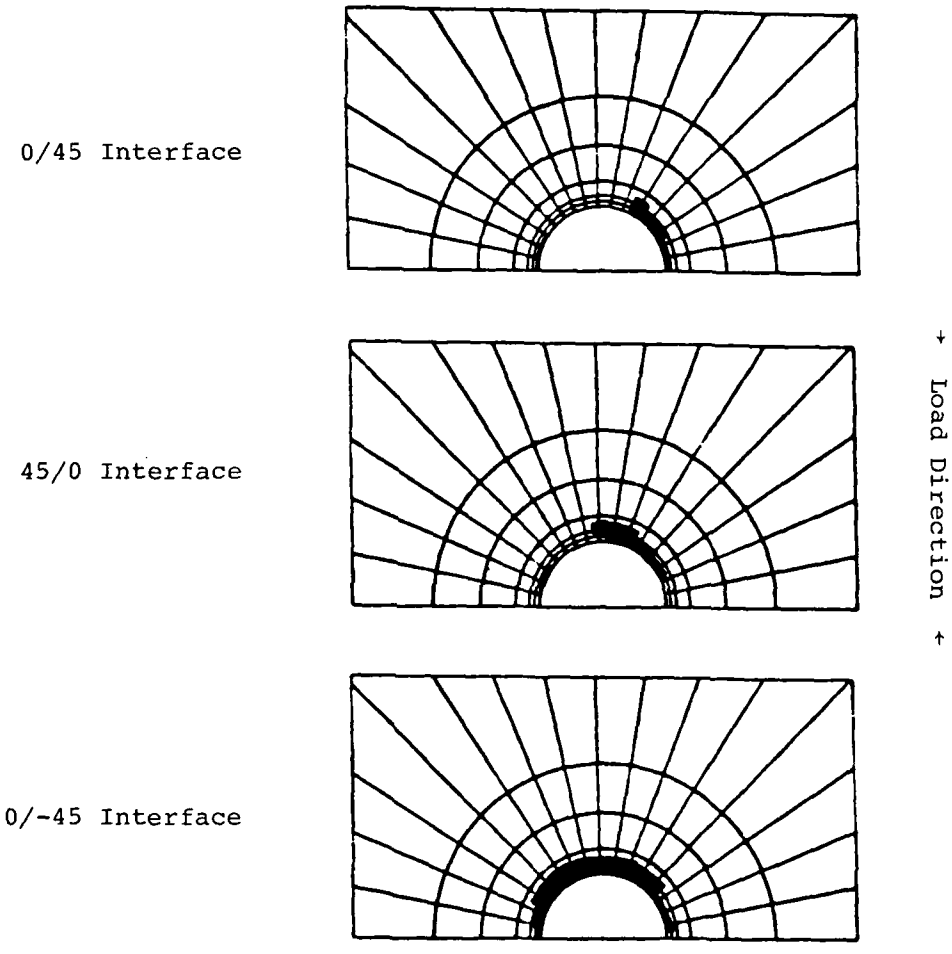

Figure 21. Interlaminar Damage in $[0/45/0/-45]_s$ - 5209 for a Load of 31.9 ksi

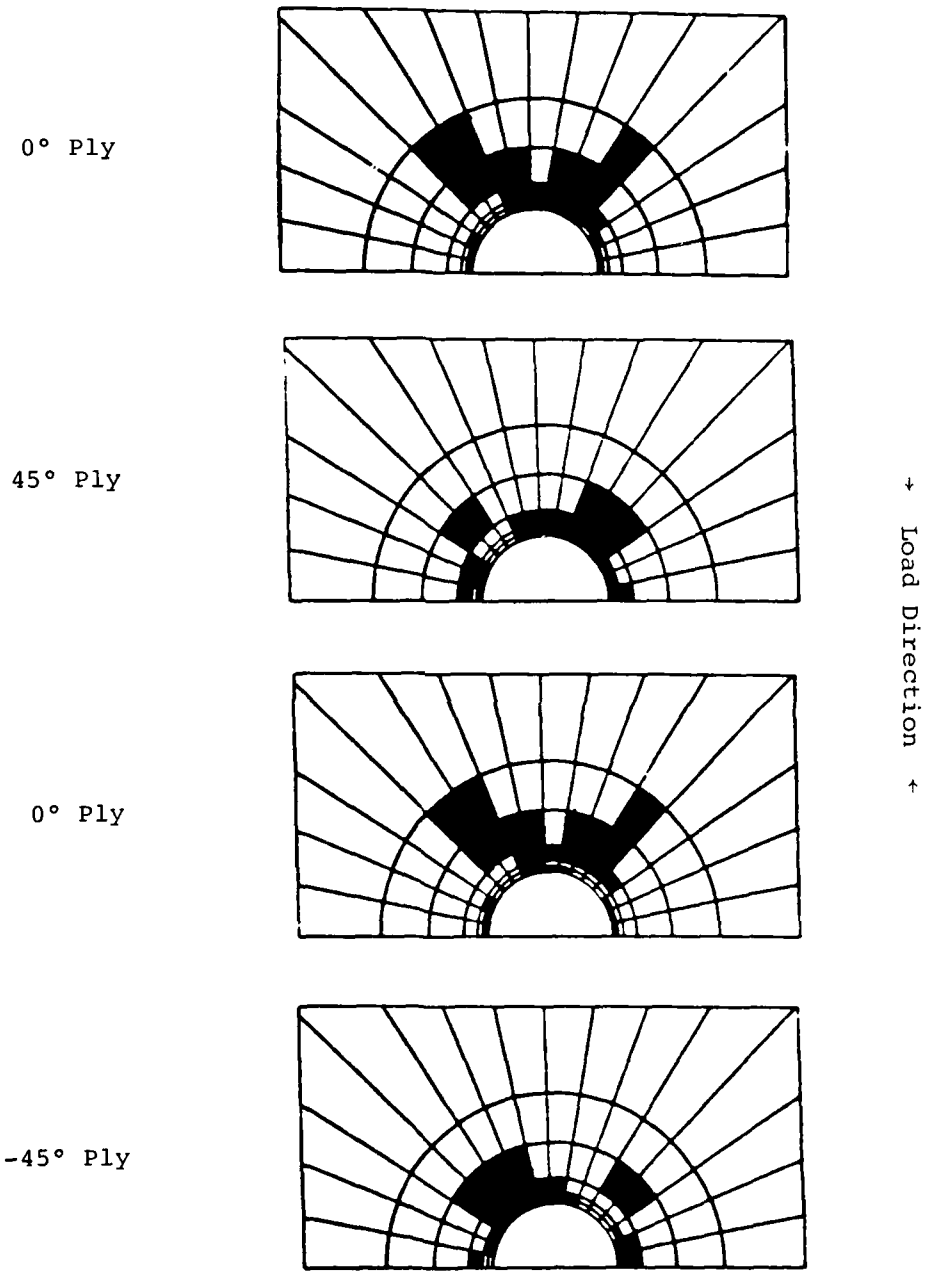

Figure 22. Intralaminar Damage in $[0/45/0/-45]_s$ - 5208 for a Load of 35.7 ksi

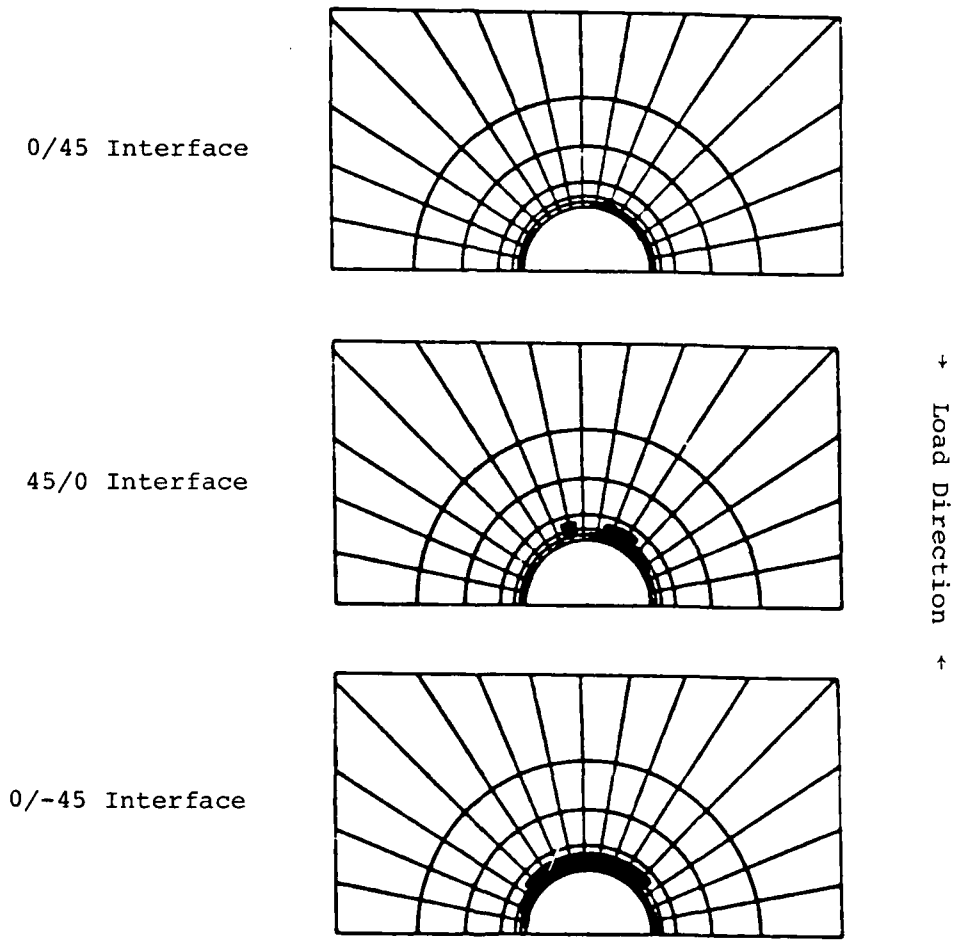

Figure 23. Interlaminar Damage in $[0/45/0/-45]_s$ - 5208 for a Load of 35.7 ksi

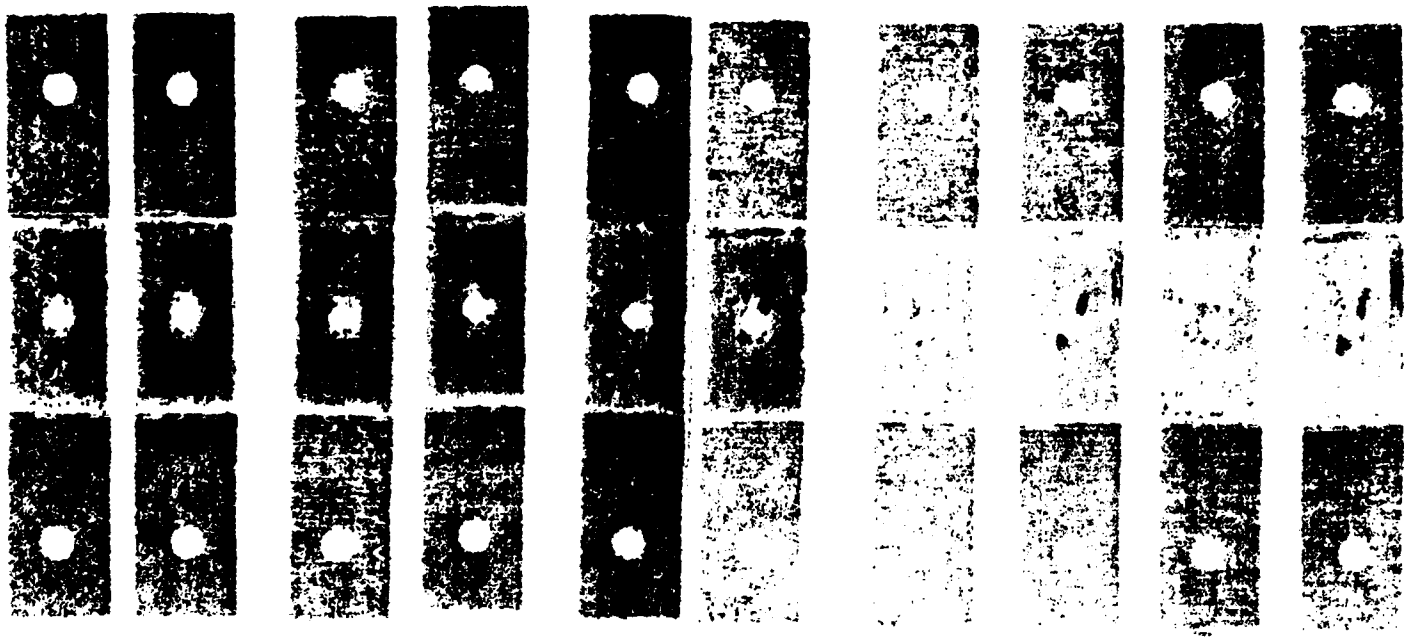

Figure 24. C-scans of Specimen 8-B-9 $[0/45/0/-45]_{5s}$ - 5208. at Different Load Cycle Levels

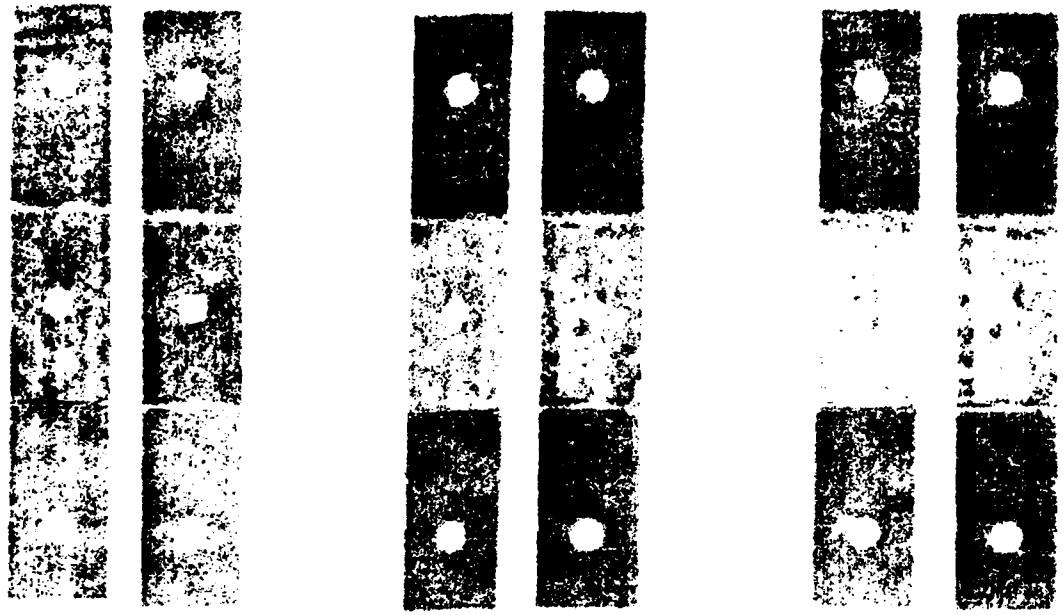

Figure 25. C-scans of Specimen 9-B-11 $[0/45/0/-45]_{5s}$ - 5209 at Different Load Cycle Levels

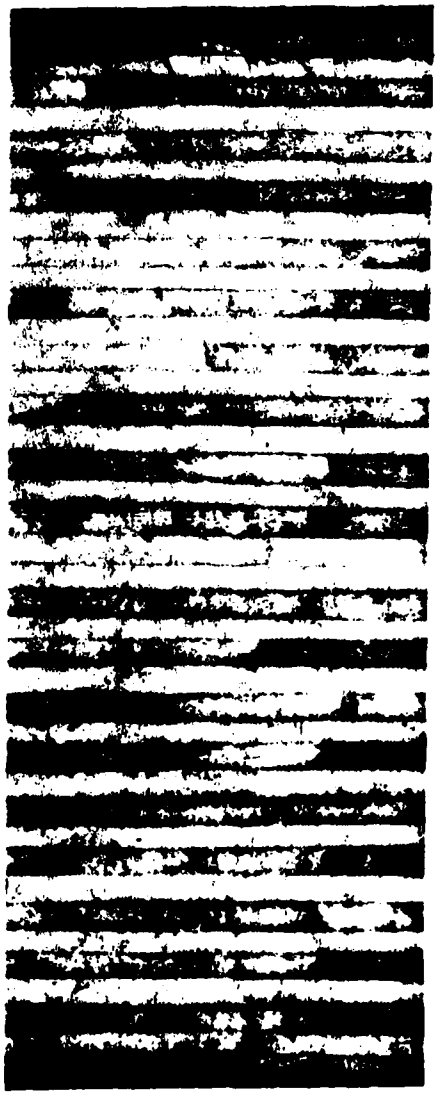

Figure 26. Transverse Section of Specimen 9-B-8 $[0/45/0/-45]_{5s}$ - 5209 at Different Load Cycle Levels

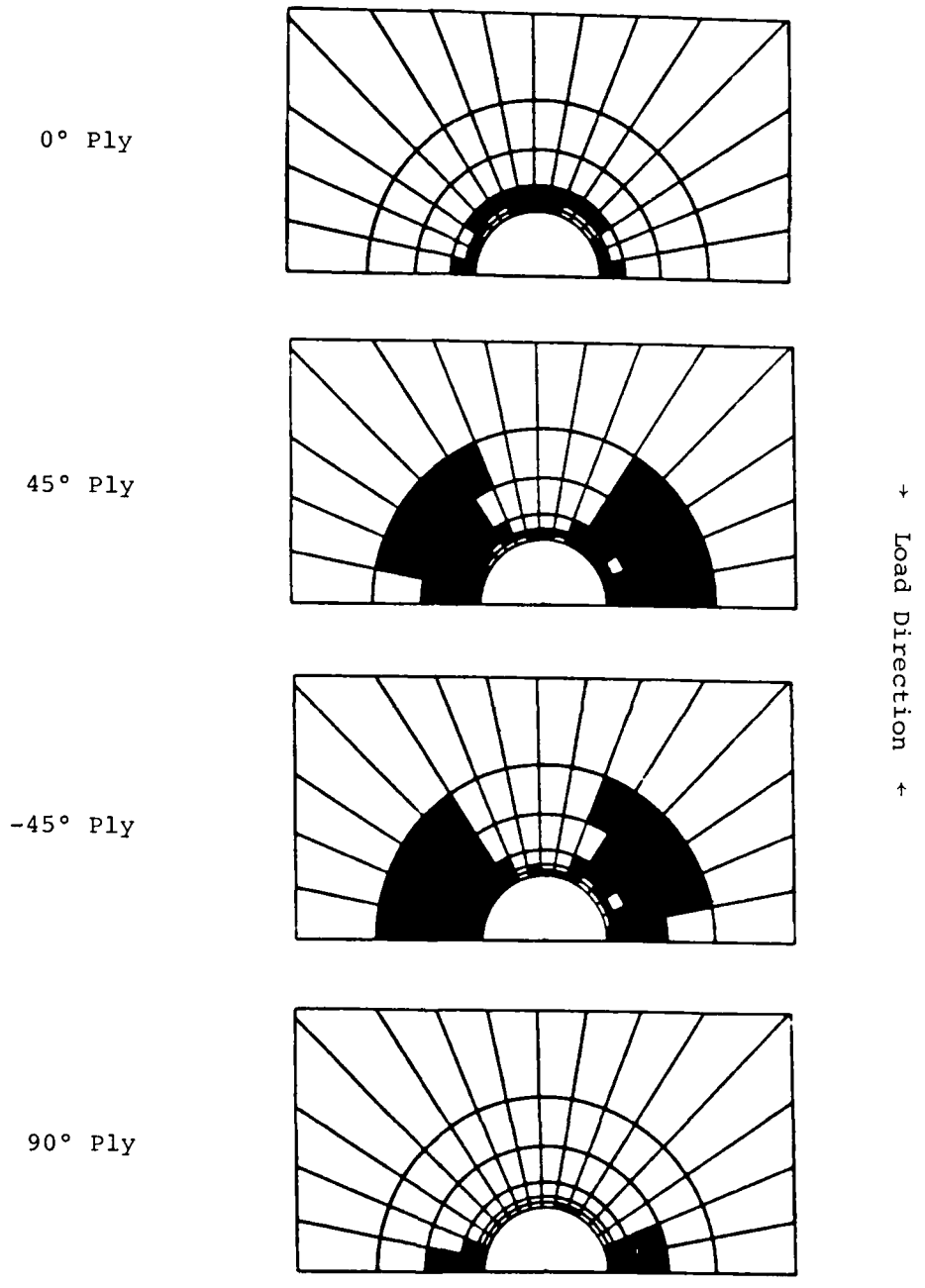

Figure 27. Intralaminar Damage in $[0/\pm45/90]_s$ - 5208 for a Load of 41.7 ksi

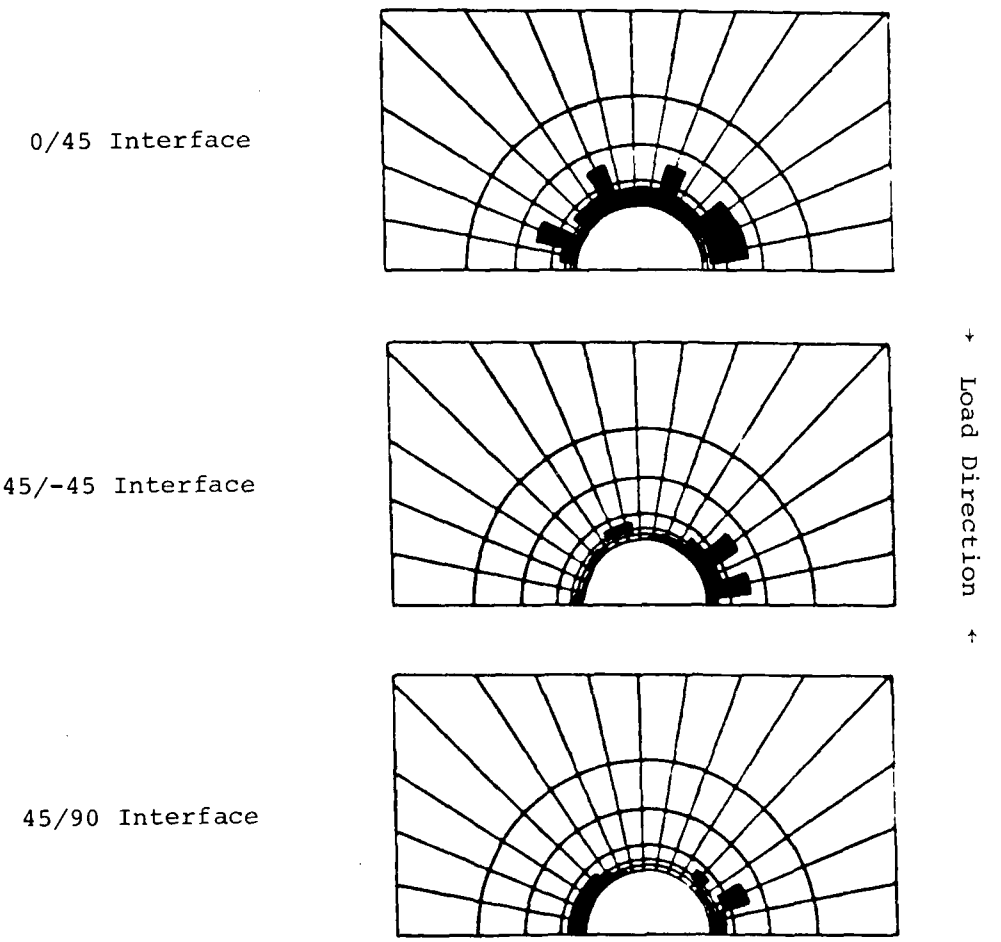

Figure 28. Interlaminar Damage in $[0/\pm 45/90]_s$ - 5208 for a Load of 41.7 ksi

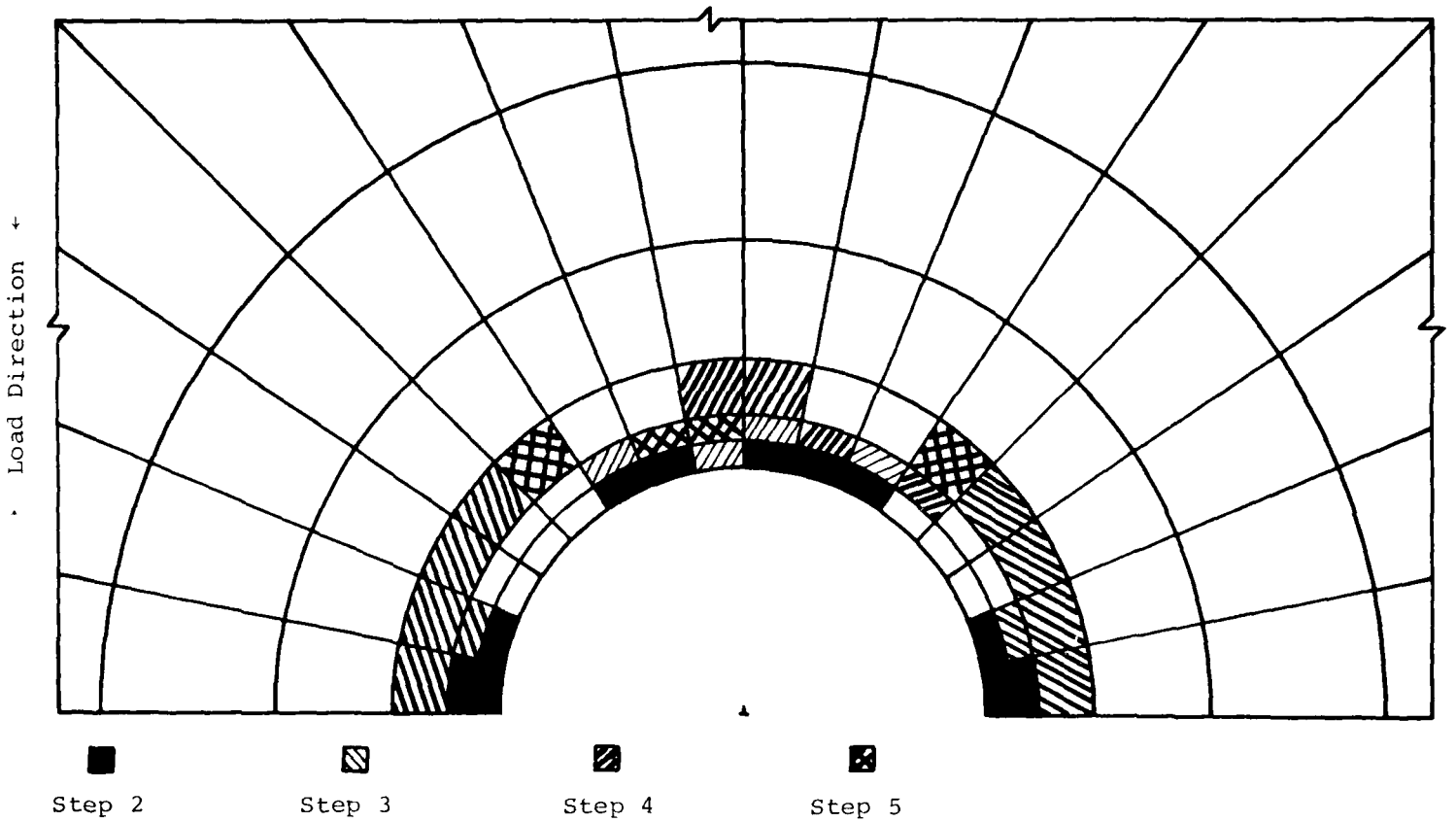

Figure 29. Interlaminar Damage Growth in $[0/\pm45/90]_s$ - 5208 for a Five Step Analysis Final Load of 41.7 ksi

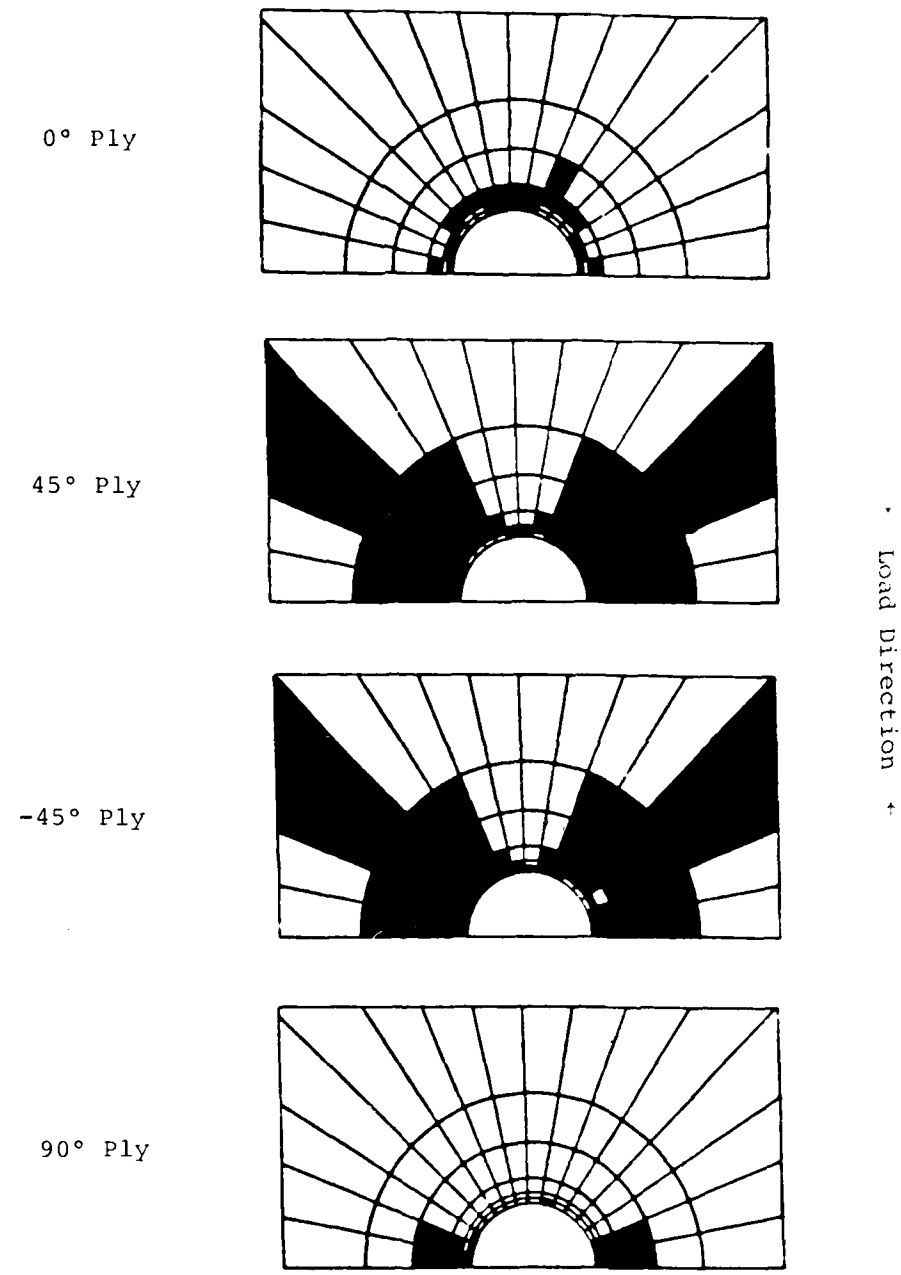

Figure 30. Intralaminar [illegible] - 5209
for a Load [illegible]

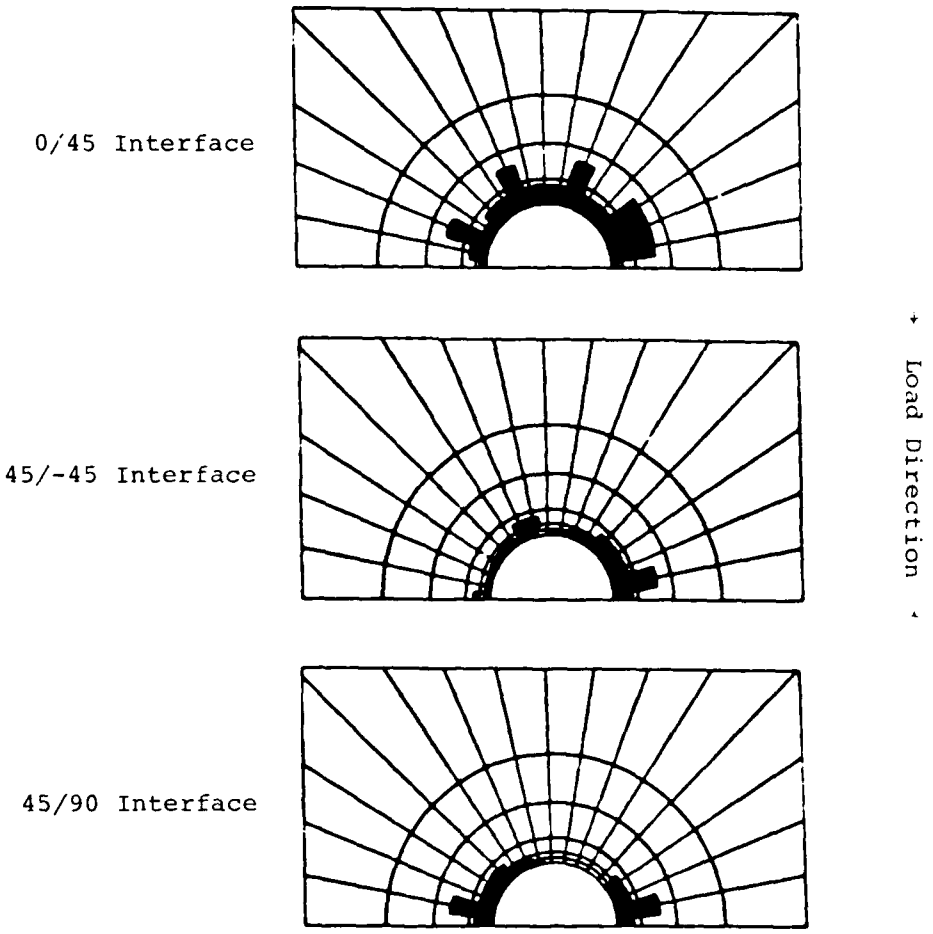

Figure 31. Interlaminar Damage in $[0/\pm45/90]_s$ - 5209 for a Load of 44 ksi

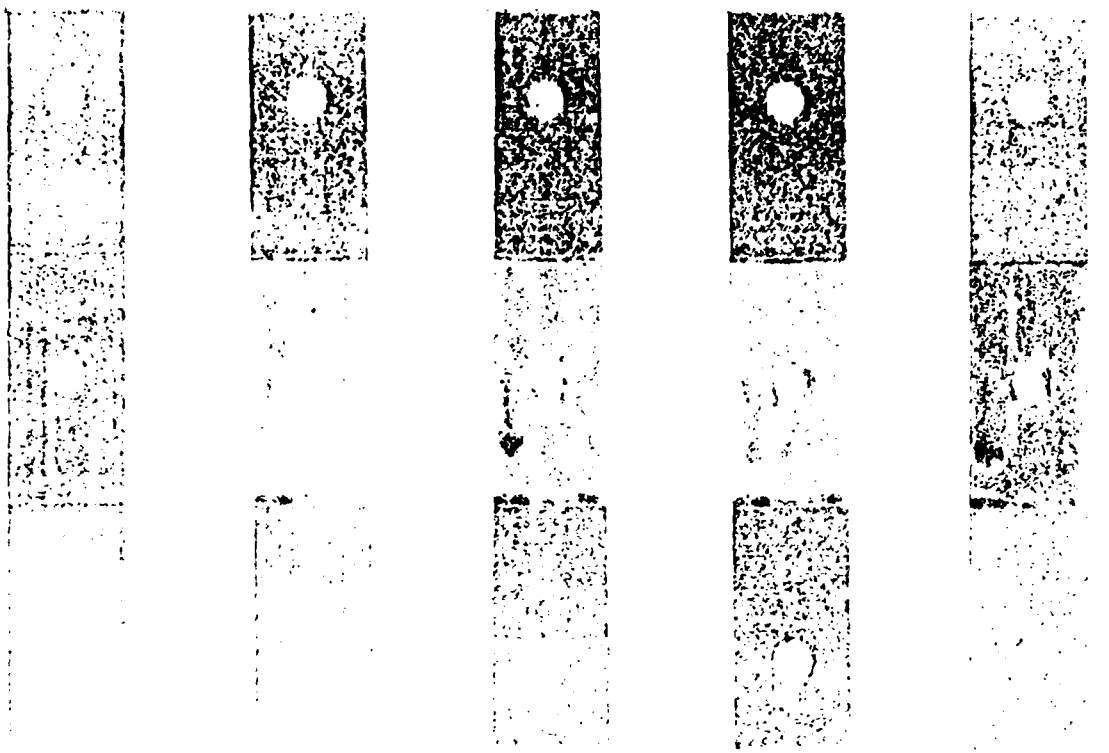

Figure 32. C-scans of Specimen 3-C-13 $[0/\pm45/90]_{5s}$ - 5208 at Different Load Cycle Levels

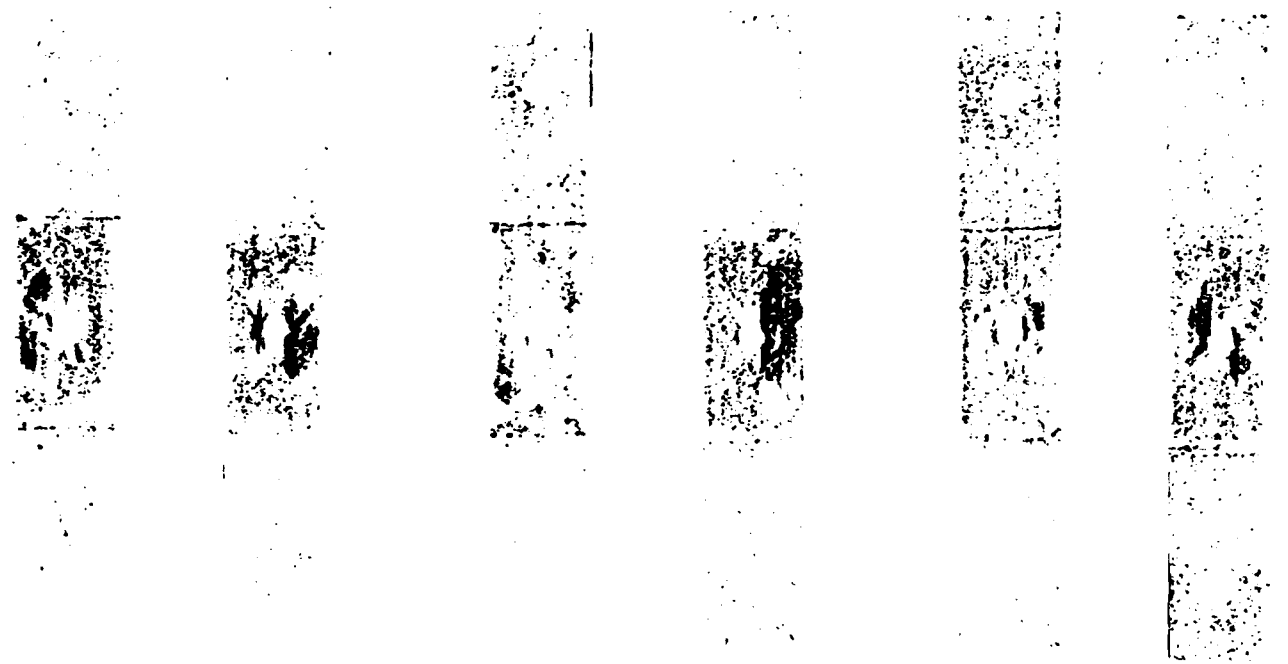

Figure 33. C-scans of Specimens 8-C-12, 8-C-13, 8-C-14 $[0/\pm45/90]_{5s}$ - 5208 After a Million Cycles

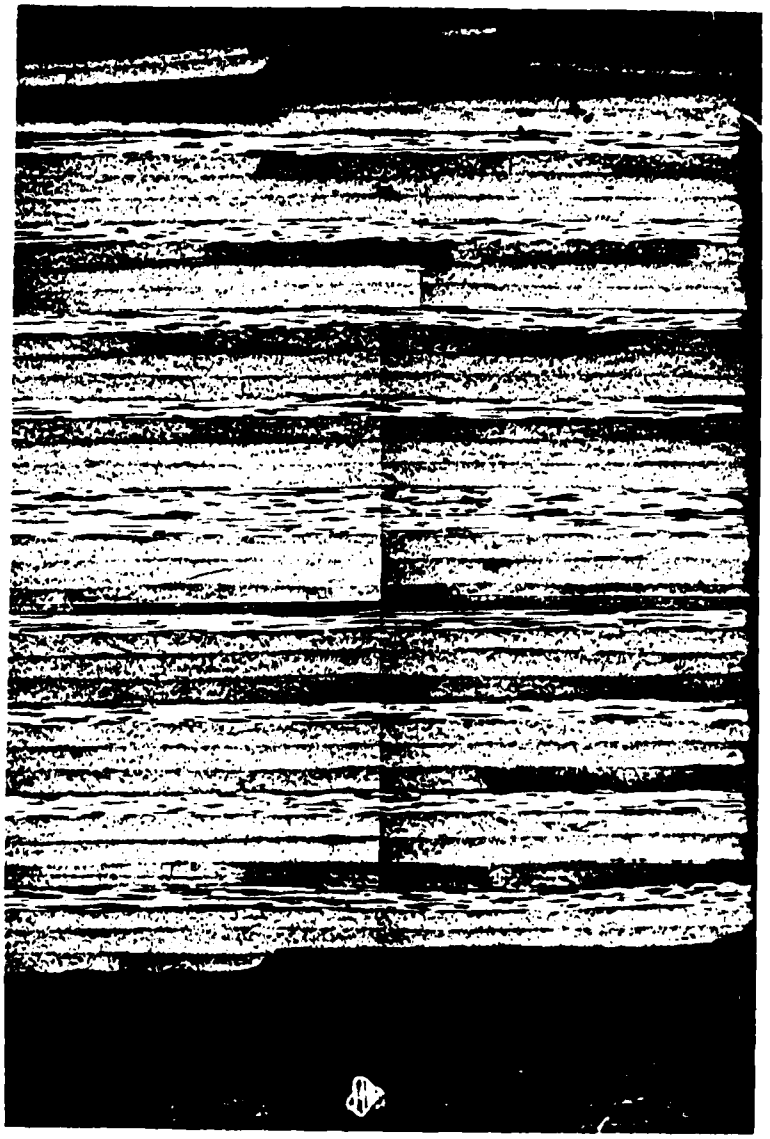

Figure 34. Transverse Section of Specimen 8-C-14 $[0/\pm45/90]_{5s}$ - 5208

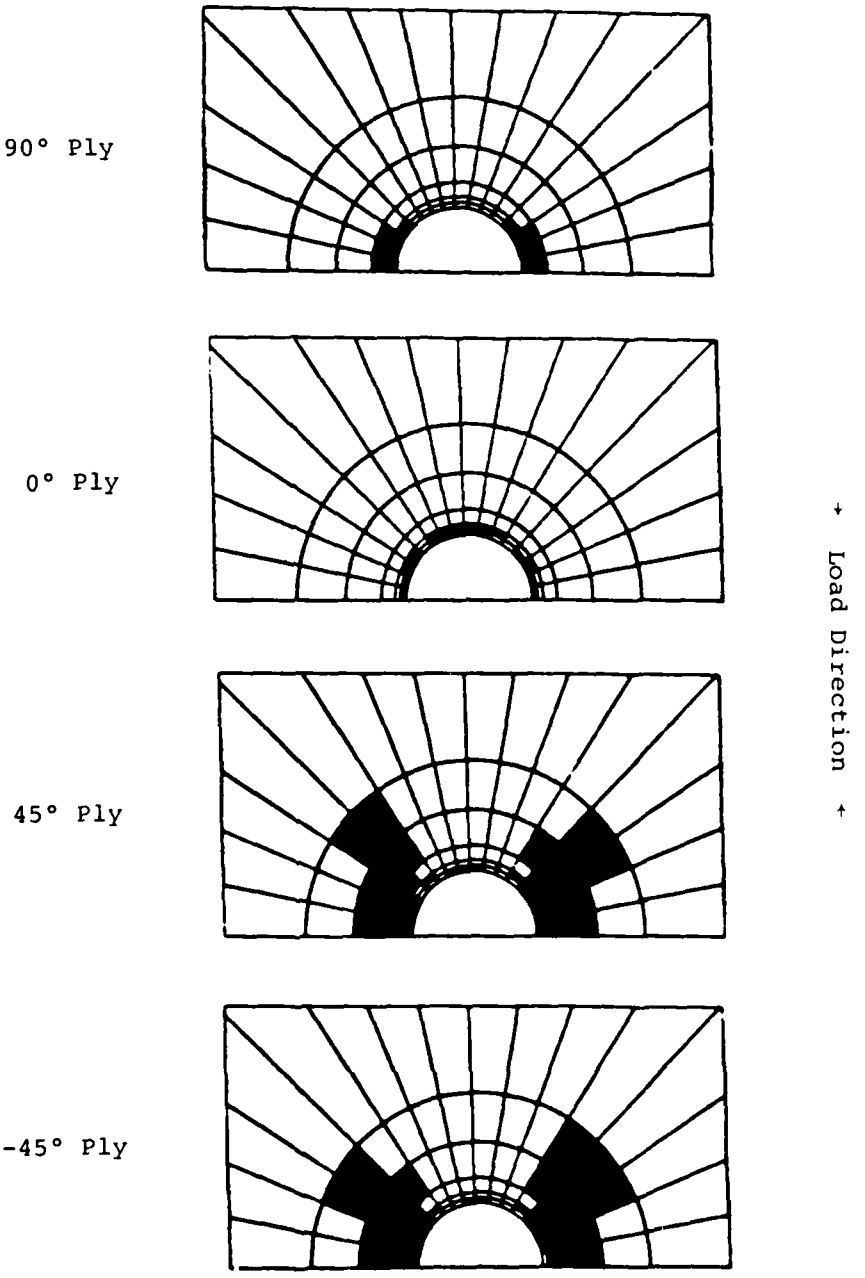

Figure 35. Intralaminar Damage in $[90/0/\pm45]_s$ - 5208 for a Load of 17.8 ksi

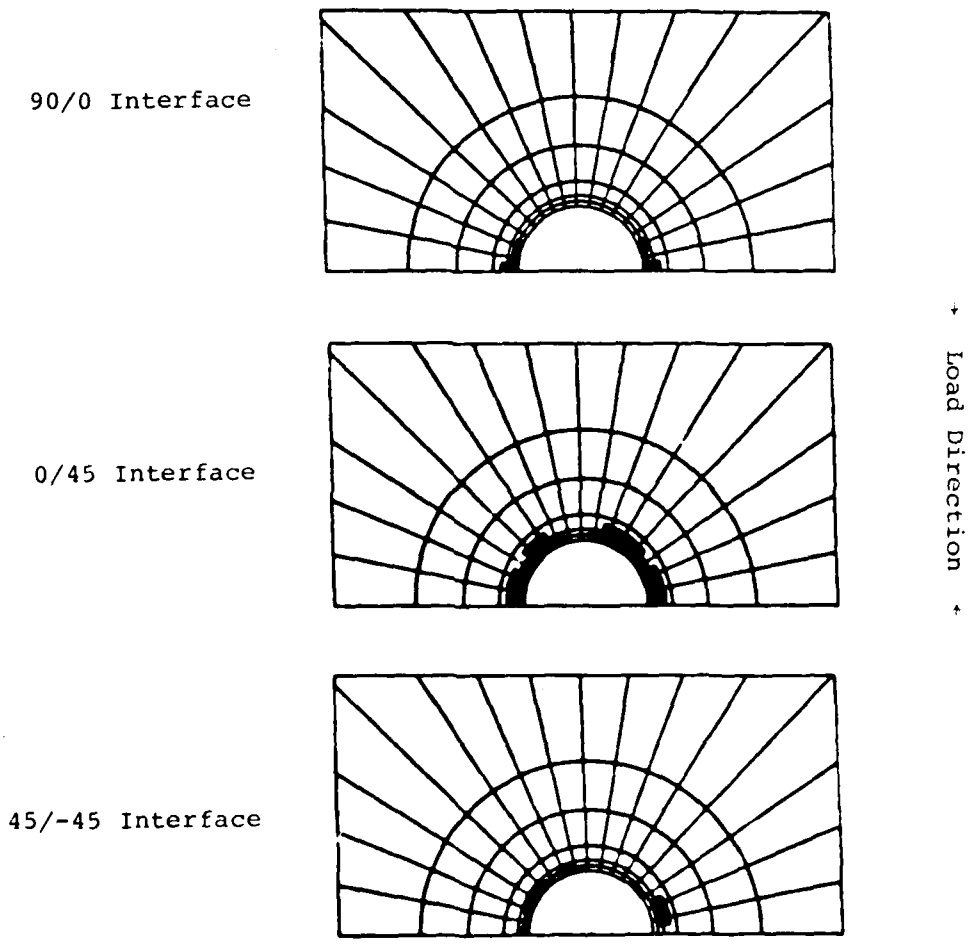

Figure 36. Interlaminar Damage in $[90/0/\pm 45]_s$ - 5208 for a Load of 17.8 ksi

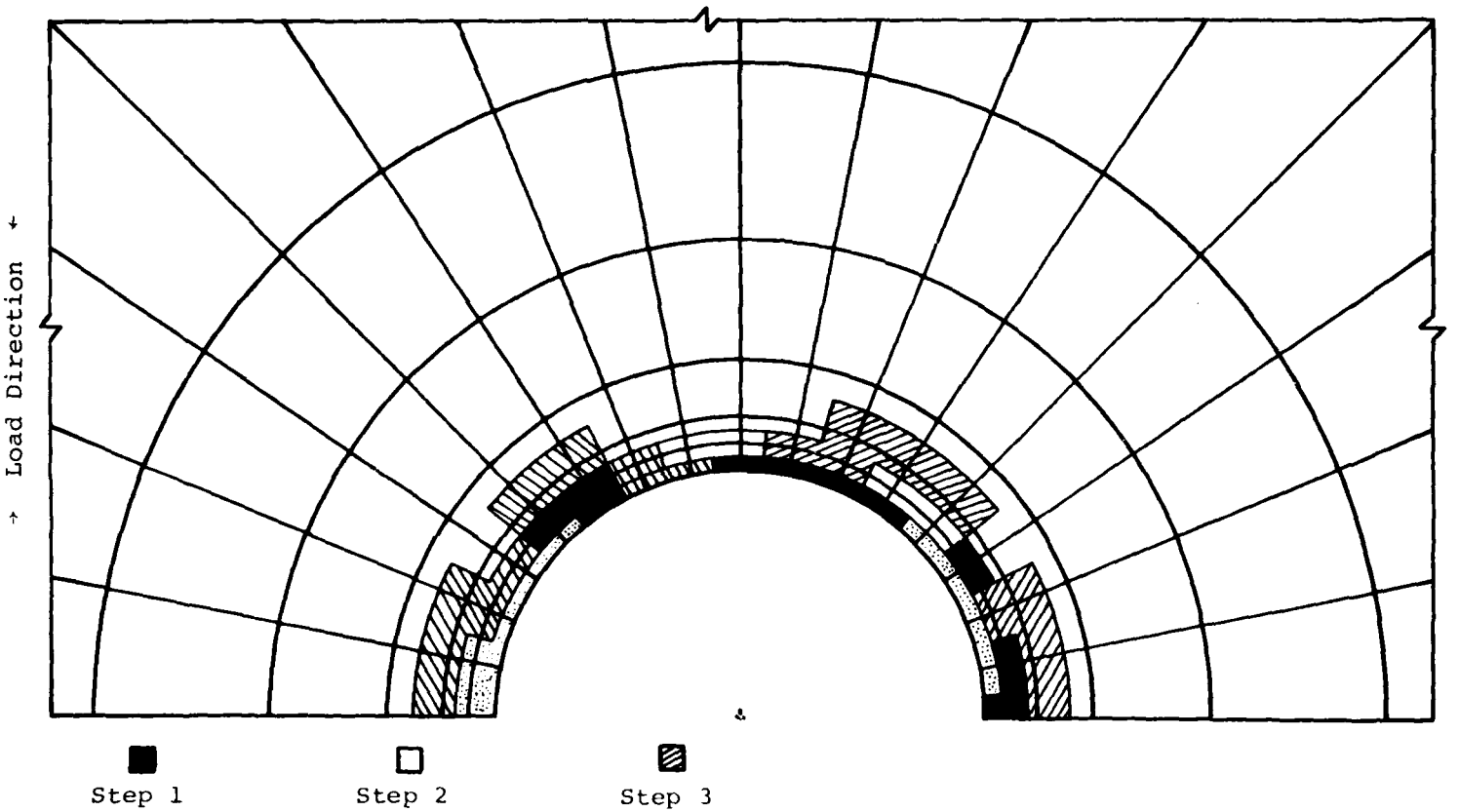

Figure 37. Interlaminar Damage Growth in $[90/0/\pm45]_s$ - 5208 for a Five Step Analysis Final Load of 17.8 ksi

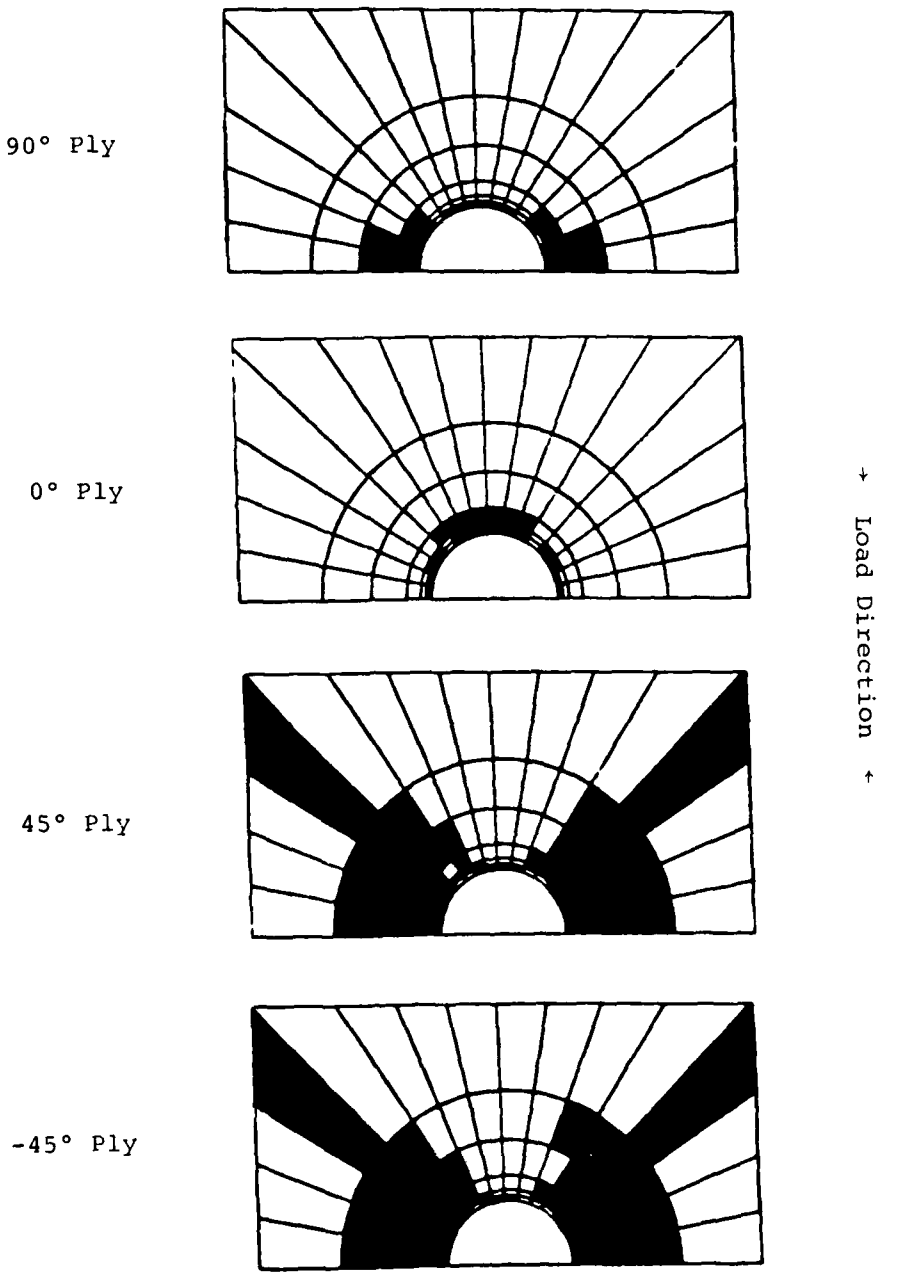

Figure 38. Intralaminar Damage in $[90/0/\pm 45]_s$ - 5209 for a Load of 21.3 ksi

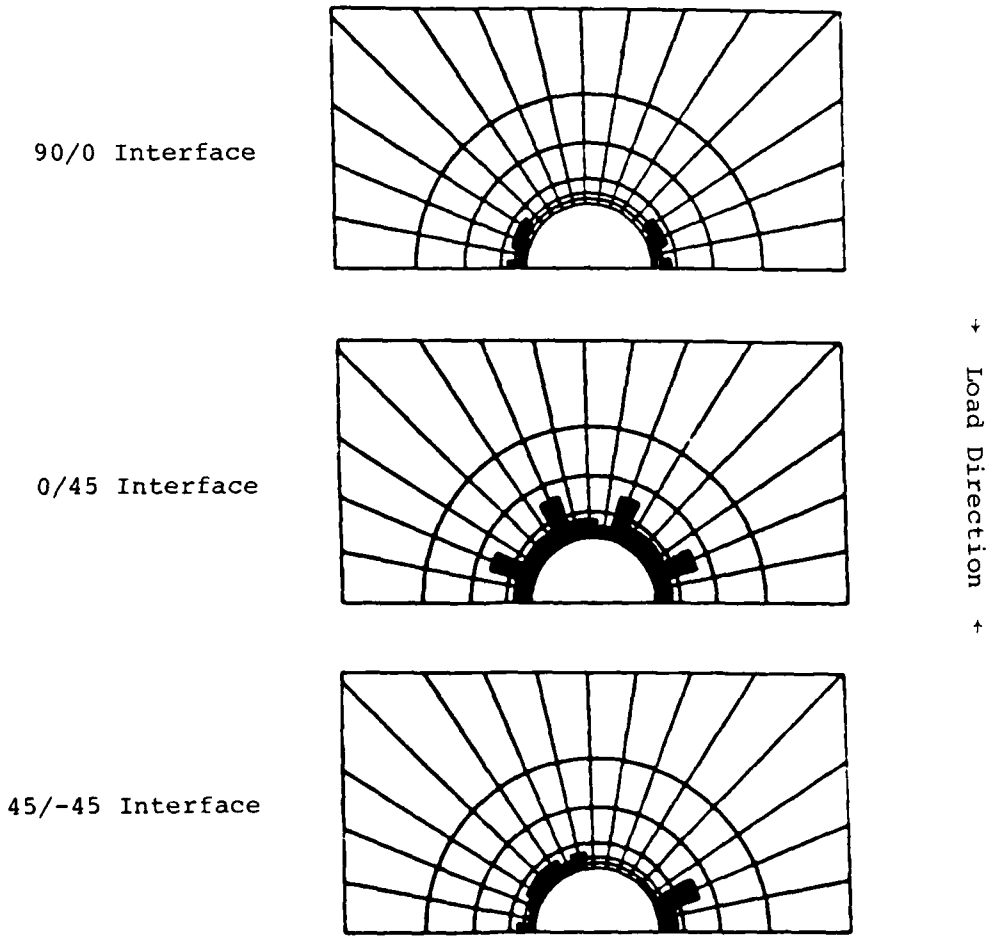

Figure 39. Interlaminar Damage in $[90/0/\pm45]_s$ - 5209 for a Load of 21.3 ksi

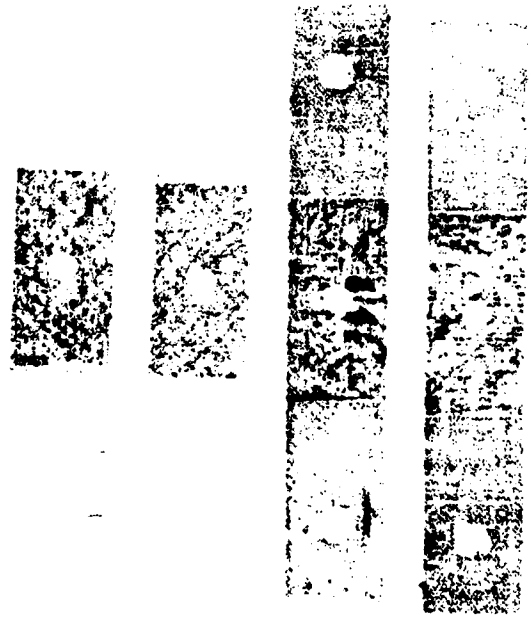

Figure 40. C-scans of Specimen 8-D-10 $[90/0/\pm45]_{5s}$ - 5208 at Different Load Cycle Levels

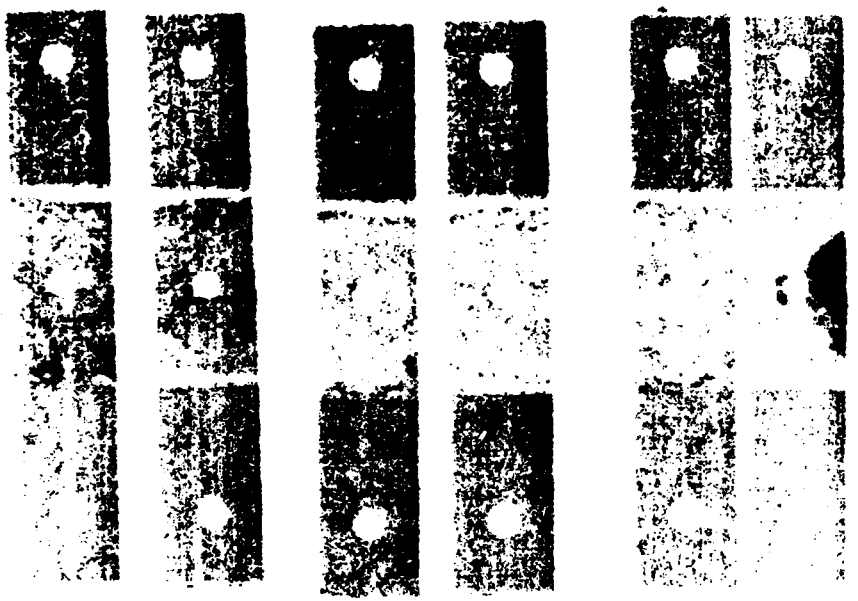

Figure 41. C-scans of Specimen 9-D-11 $[90/0/\pm45]_{5s}$ - 5209 at Different Load Cycle Levels

Figure 42. Axial Section of Specimen 9-D-11 $[90/0/\pm45]_{5s}$ - 5209

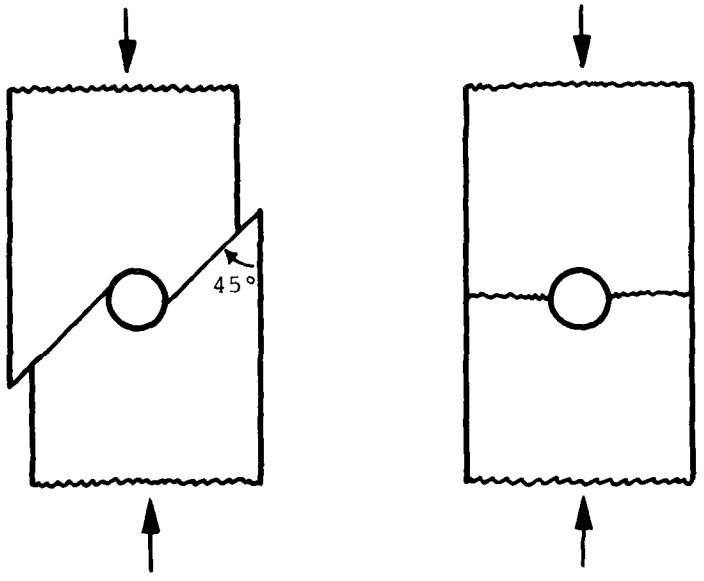

Figure 43. Notched Compression Failure Modes

AD-A113 654 MATERIALS SCIENCES CORP SPRING HOUSE PA F/G 11/4
RESEARCH STUDY TO DEFINE THE CRITICAL FAILURE MECHANISMS IN NOT--ETC(U)
MAR 81 B W ROSEN, A P NAGARKAR, R B PIPES N00019-79-C-0633
UNCLASSIFIED MSC/TFR/1201/1801 NL

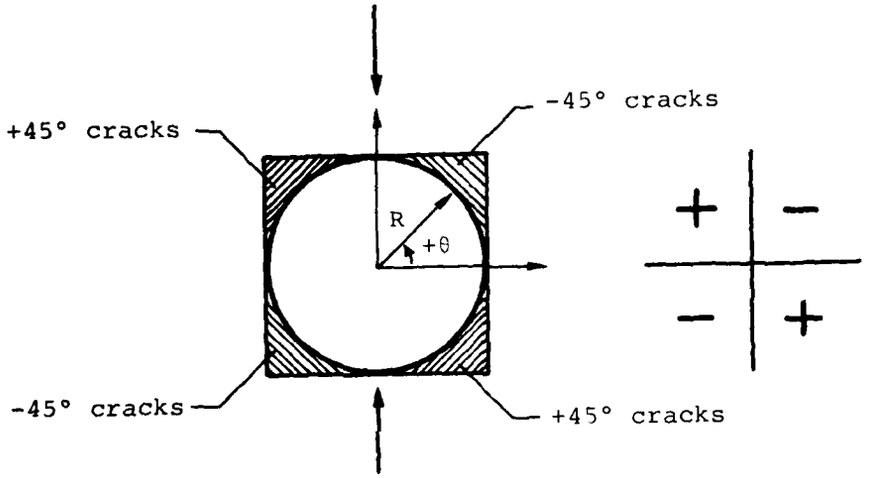

Figure 44. Fatigue Crack Pattern and Cracked Laminae by Quadrant

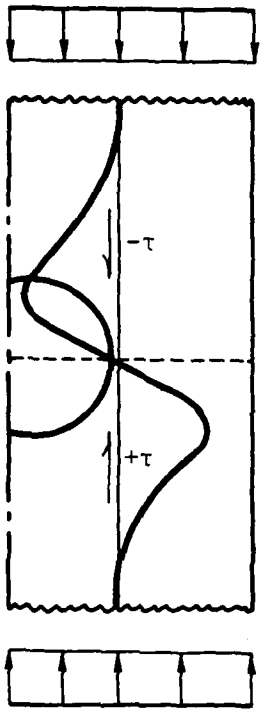

Figure 45. Antisymmetric Distribution of the Shearing Stress, τ

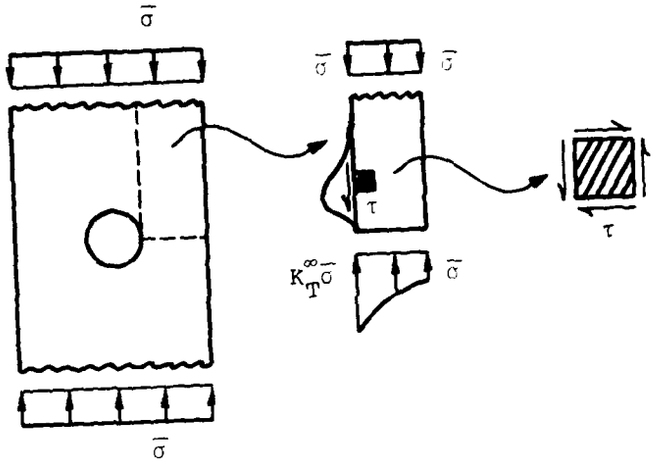

Figure 46. Direction of the Shearing Stress, τ

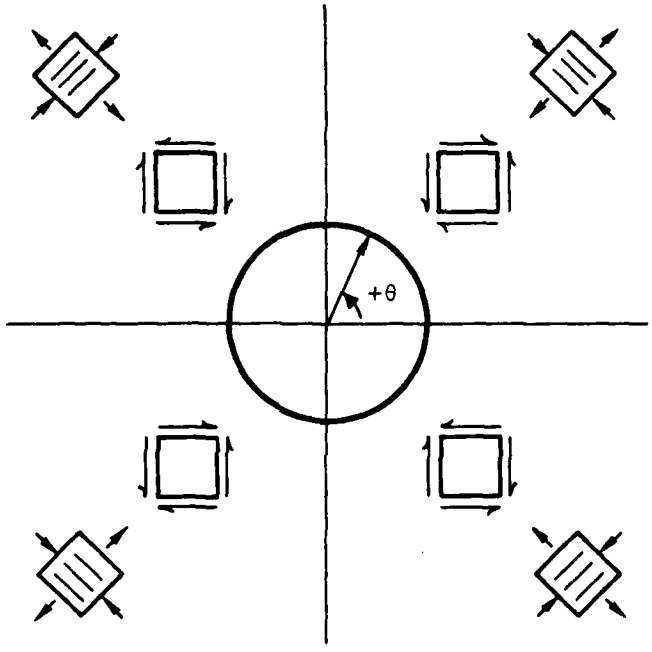

Figure 47. Shear Induced Transverse Tensile Stresses

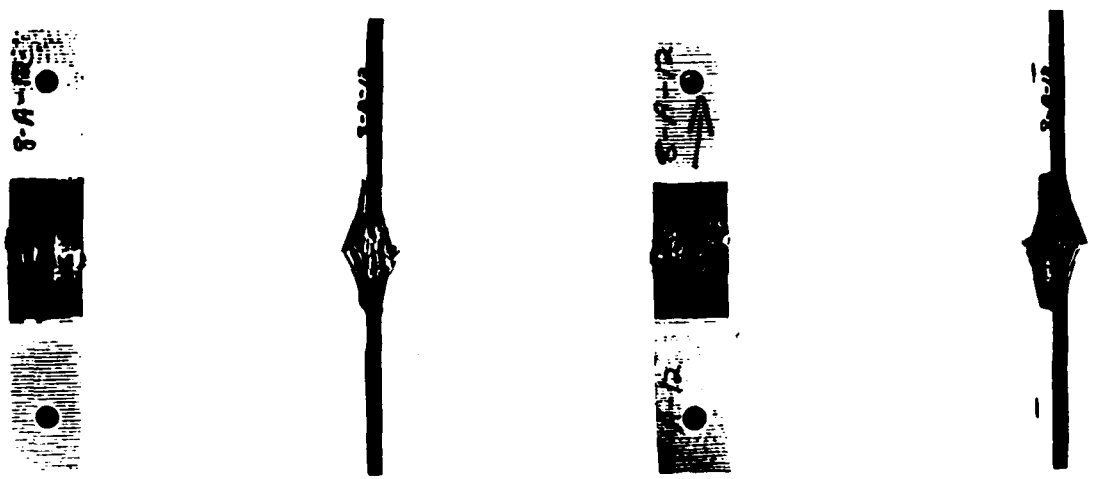

Figure 48. Residual Strength Failure - Specimen 8-A-12

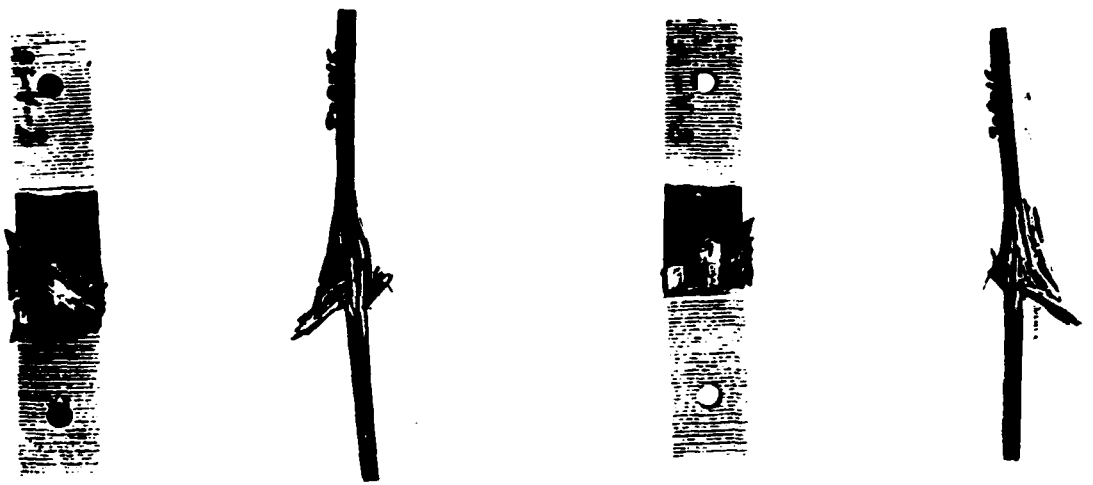

Figure 49. Static Unnotched Failure - Specimen 8-A-16

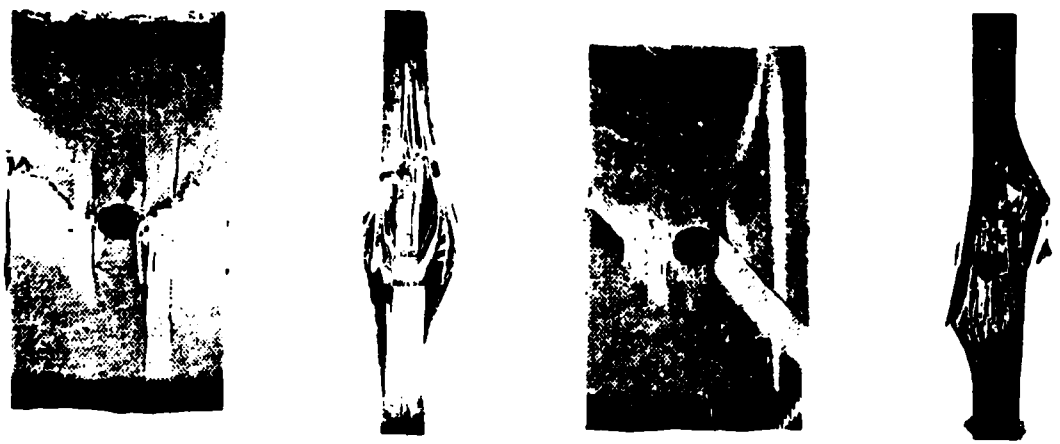

Figure 50. Residual Strength Failure - Specimen 9-B-12

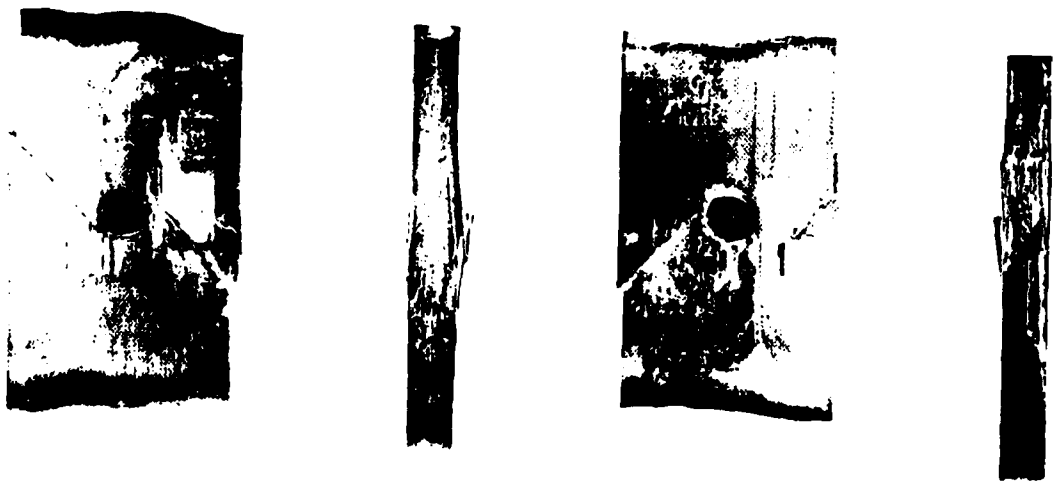

Figure 51. Residual Strength Failure - Specimen 9-B-4

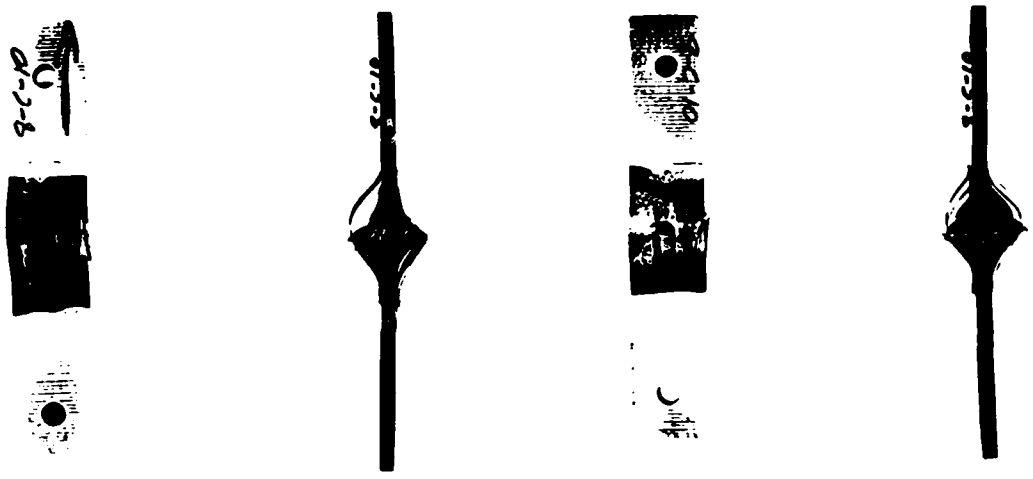

Figure 52. Residual Strength Failure - Specimen 8-C-10

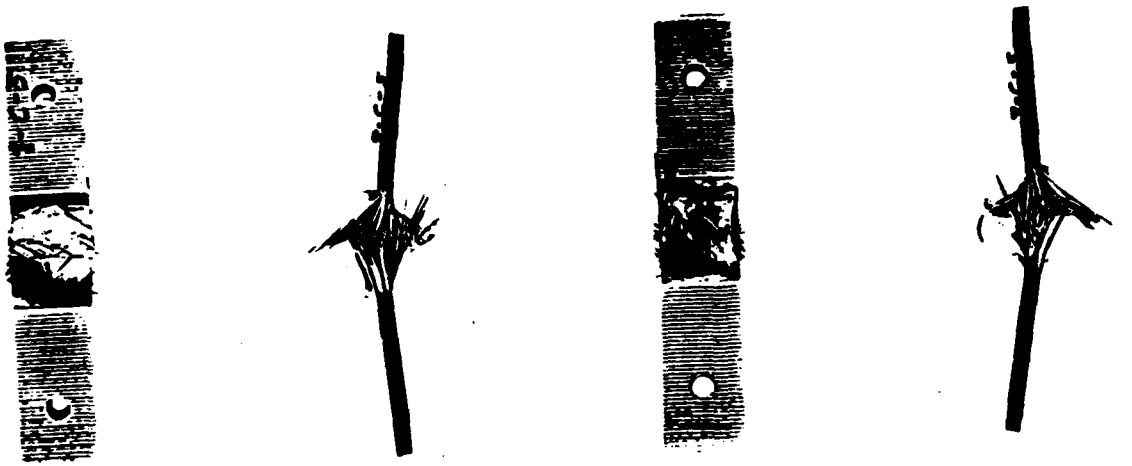

Figure 53. Static Unnotched Failure - Specimen 8-C-5

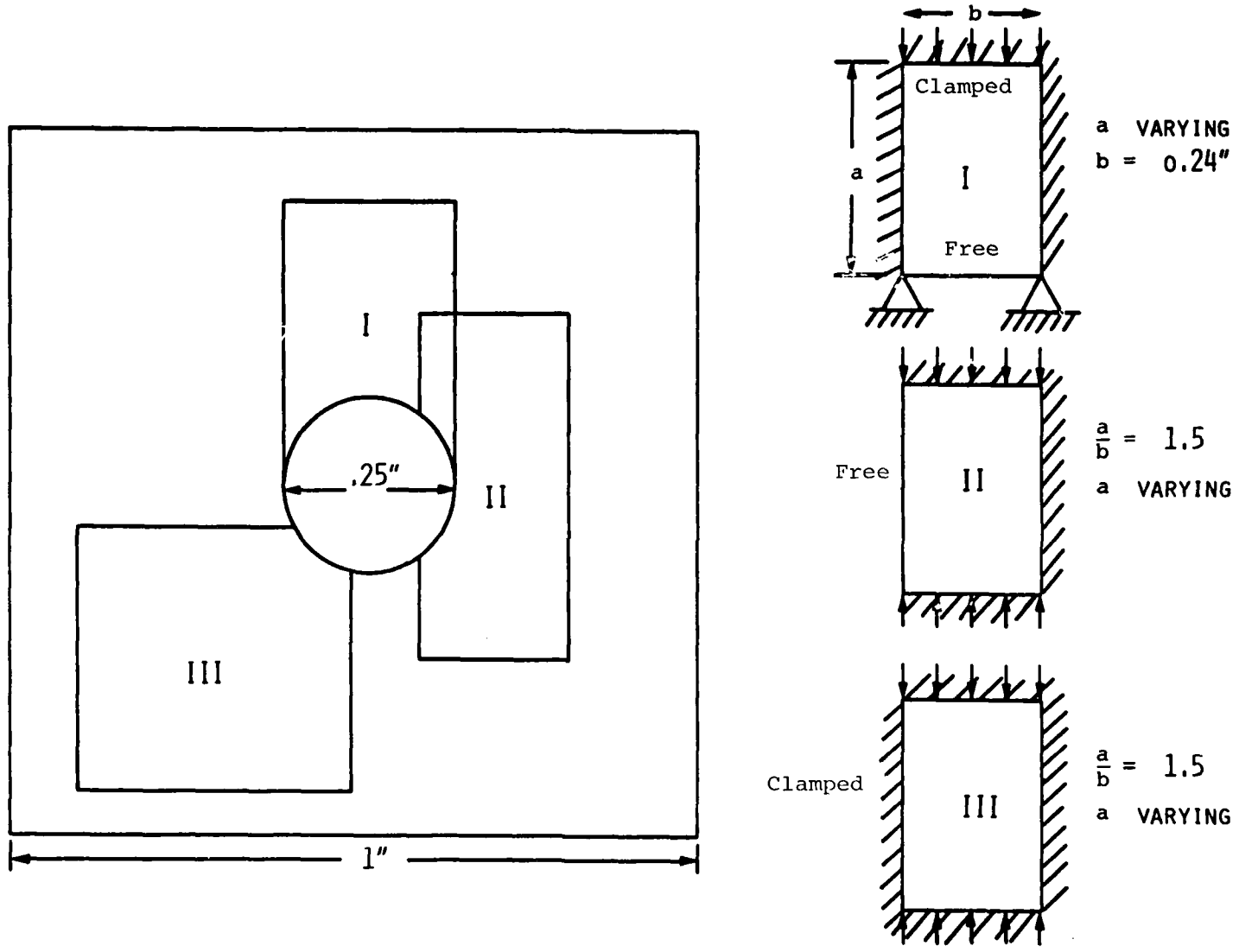

Figure 54. Buckling of Delaminated Plies

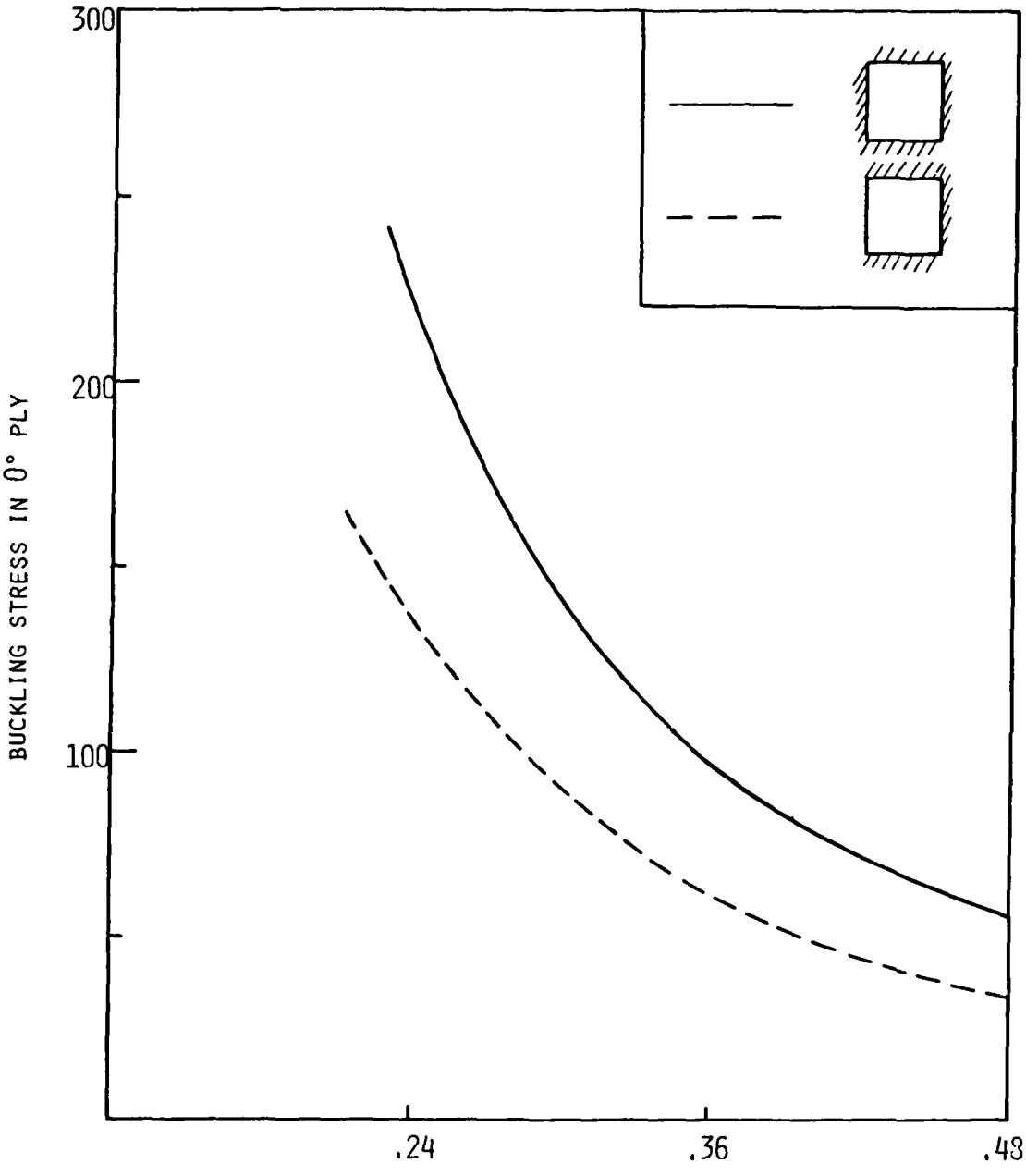

Figure 55. Calculated Surface Ply Buckling Stresses

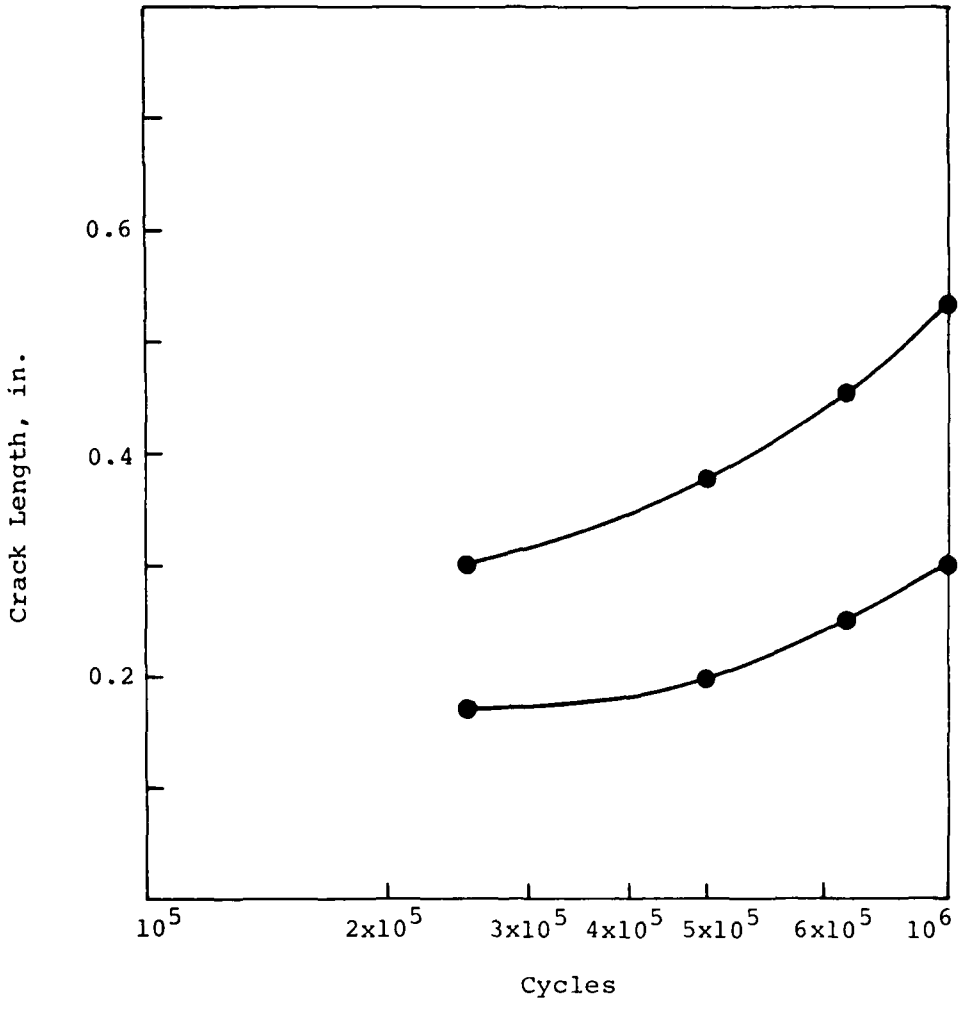

Figure 56. Delamination Crack Growth in Load and Transverse Direction in a Quasi-isotropic Laminate

Distribution List for Final Report

	No. of Copies
Naval Air Systems Command Washington, DC 20361	11
2 for AIR-950D 3 for AIR-320B 3 for AIR-5304 and 3 for AIR-5302	
Naval Air Development Center Warminster, PA 18974	5
ATTN: Code 6043, Mr. P. Kozel Code 6043, Dr. S. L. Huang Code 6043, Mr. T. Hess Code 6043, Mr. L. Gauss Code 606 , Dr. J. Deluccia	
Naval Sea Systems Command Washington, DC 20362	3
ATTN: Code 05R15, Dr. H. Vanderveldt Code 062R4, Mr. M. Kinna Code 03R24, Mr. J. Gagorik	
Office of Naval Research Arlington, VA 22217	2
ATTN: Code 474, Dr. N. Perrone Code 471, Dr. B. McDonald	
Naval Ship R&D Center Bethesda, MD 20034	1
ATTN: Code 173.2, Mr. Couch	
Naval Ship R&D Center Annapolis, MD 21401	1
ATTN: Mr. J. Gudas	
Naval Surface Weapons Center White Oak, MD 20910	1
ATTN: Mr. J. Agul	
Naval Research Laboratory Washington, DC 20375	2
ATTN: Dr. I. Wolock, Code 6383 Dr. G. Yoder, Code 6384	
Wright Aero Labs AFFDL Wright Patterson AFB, OHIO 45433	3
ATTN: Mr. P.A. Parmley Mr. G.P. Sendeckji Mr. G.E. Maddux	

Distribution List for Final Report (continued)

Wright Aero Labs, AFML 2
Wright Patterson AF Base, OHIO 45433

ATTN: Mr. T.G. Reinhard, Jr.
Mr. G.P. Peterson

Air Force Office of Scientific Research 2
Bldg. 410 Bolling AFB
Washington, DC 20332

ATTN: Dr. A. Amos
Dr. M. Salkind

Defense Advanced Research Project Agency 1
1400 Wilson Blvd.
Arlington, VA 22209

ATTN: Dr. E.C. VanReuth

Army Air Mobility R&D Laboratory 1
Fort Eustis, VA 23604

ATTN: Mr. H. Reddick

NASA 3
Langley Research Center
Hampton, VA 23365

ATTN: Dr. J. Davidson
Dr. R. Pride
Dr. G.L. Roderick

Army Materials & Mechanics Research Center 2
Watertown, MA 02172

ATTN: Dr. E. Lenoe
Mr. D. Oplinger

Army Mobility R&D Lab., Ames Research Center 1
Moffett Field, CA 94035

ATTN: Dr. Raymond Foye

Army Research Office 1
Research Triange Park, NC 27709

ATTN: Dr. F. Schmiedeshoff

Distribution List for Final Report (continued)

McDonnell Douglas Corporation 5
McDonnell Aircraft Company
P.O. Box 516
St. Louis, MO 63166

ATTN: Mr. K. Stenberg
Mr. R. Riley
Mr. R. Garrett
Dr. D. Ames
Dr. C. Whitsett

Northrop Corporation 3
3901 W. Broadway
Hawthorne, CA 90250

ATTN: Dr. N. Bhatia
Dr. L. Jeans
Dr. M. Ratwani

General Dynamics/CONVAIR Division 1
P.O. Box 80847
San Diego, CA 92138

ATTN: Mr. W. Scheck

General Dynamics 2
Aerospace Division
P.O. Box 748
Ft. Worth, TX 76101

ATTN: Dr. R. Wilkins
Mr. S. Manning

Lockheed Missiles & Space Co. 1
Sunnyvale, CA 94088

ATTN: Mr. H. Marshall

Vought Corporation 3
Advanced Technology Center
Dallas, TX 75266

ATTN: Dr. J. Renton
Mr. E. Donahu
Dr. D.H. Peterson

Grumman Aerospace Corporation 3
Bethpage, NY 11714

ATTN: Mr. R. Hadcock
Mr. S. Dastin
Mr. W. Grant

Distribution List for Final Report (continued)

Sikorsky Aircraft 1
Stratford, CT 06602

ATTN: Mr. M.J. Rich

Bell Helicopter 1
P.O. Box 482
Fort Worth, TX 76101

ATTN: Mr. J. McGuigan

Hughes Helicopters 1
Centinela and Teale St.
Culver City, CA 90230

ATTN: Mr. G. Rock

Boeing Vertol Co. 1
Philadelphia, PA 19142

ATTN: Mr. R. Peck

Kaman Aerospace Corporation 1
Old Windsor Road
Bloomfield, CT 06002

ATTN: Mr. J. Schauble

Rockwell International Corp./Science Center 2
P.O. Box 1085
1049 Camino Dos Rios
Thousand Oaks, CA 91360

ATTN: Dr.Neil Paton
Ms. R. Richards

Pratt & Whitney Aircraft 1
Division of United Aircraft Corporation
Florida Research & Development Ctr.
P.O. Box 2691
West Palm Beach, FL 33402

ATTN: Mr. John Miller

The Franklin Institute Research Laboratories 1
Twentieth & Parkway
Philadelphia, PA 19103

ATTN: Technical Director